

Deep Learning Decision Support System for Open-Pit Mining Optimisation: GPU-Accelerated Planning Under Geological Uncertainty

Iman Rahimi

Faculty of Engineering & Information Technology, University of Technology Sydney,
Australia

Abstract- This study presents a unified AI-enhanced Decision Support System (DSS) for long-term open-pit mine planning that simultaneously addresses geological realism, large-scale computational complexity, and operational decision uncertainty. The framework introduces a Variational Autoencoder (VAE) for dynamic geological scenario generation that preserves spatial correlations and grade-tonnage relationships, overcoming the limitations of static scenario sets commonly used in stochastic mine planning. A spatially-aware uncertainty propagation model combines variogram-based geostatistics, temporal confidence evolution, and geological features to produce risk-adjusted economic evaluations. To solve the resulting large-scale, uncertainty-rich optimization problem, we develop a hybrid metaheuristic architecture integrating Genetic Algorithms, Large Neighbourhood Search, Simulated Annealing, and an enhanced Dantzig–Wolfe decomposition capable of generating complete mining sequences conditioned on VAE-generated geological realizations. These algorithms are coupled with multi-agent reinforcement learning for adaptive parameter control and operational decision guidance. A GPU-accelerated parallel evaluation engine supports simultaneous assessment of over 250,000 candidate moves, enabling real-time feasibility repair and scalable optimization for block models exceeding 50,000 mining units. Computational experiments demonstrate that the proposed DSS achieves up to 1.2-million-fold speed improvement over commercial MILP solvers for large instances, while consistently delivering higher expected Net Present Value under geological uncertainty. The methodology provides a robust and scalable platform for industrial-scale mine scheduling, illustrating how deep generative modelling, adaptive learning, and parallel metaheuristics can be effectively integrated to advance decision-making under uncertainty in complex operational systems.

Keywords- Decision Support System, Deep reinforcement learning, adaptive optimisation, open-pit mining, Uncertainty, Intelligent scheduling.

1. Introduction

Long-term open-pit mine planning seeks to optimize the extraction and processing sequence throughout a mine's life while managing geological, operational, and market uncertainties (Armstrong et al., 2021; Quelopana & Navarra, 2024; Tolouei et al., 2021). Metallurgical plants serve as critical components in the mineral value chain, as their efficiency directly influences the overall economic performance of mining operations. Nevertheless, complete recovery of valuable minerals such as gold and silver is rarely achievable. Attaining total extraction would require excessive use of chemical reagents, particularly cyanide, leading to higher operational expenses and diminishing overall efficiency, as some valuable minerals inevitably remain in the tailings (Ordenes J et al., 2021). Additionally, the comminution stage, which involves crushing and grinding the ore to achieve finer particle sizes (Gupta CK, 2003), is among the most energy-demanding phases of mineral processing. It typically accounts for 30%–60% of a mine's total energy consumption and can reach up to 80% in certain operations (Wang C et al., 2013; Lois-Morales P et al., 2022).

Plant reconfiguration should be treated as a strategic decision aligned with future processing requirements, not as a reaction to minor ore feed fluctuations (Navarra A et al., 2017). An operational mode represents a defined set of parameters that outline a metallurgical plant's configuration, including its metal recovery rates and processing capacities (Quelopana A et al., 2023). Each operational mode is tailored to maximize metal or alloy output while maintaining safe and efficient processing for distinct ore blends or rock types. Given the significant variability in metal grades across geological materials, operating multiple modes, where technically and economically viable, can substantially enhance plant adaptability. This operational flexibility allows for better adjustment to fluctuating ore characteristics and provides a more robust mechanism for managing uncertainty associated with grade variations (Quelopana A et al., 2023).

The surge in geological, operational, and market data demands innovative methods for efficient processing to support more accurate and adaptive mine planning. Traditional mine planning frameworks relying on deterministic models and fixed inputs fail to capture the complexity and variability of real-world geological and operational conditions. Modern approaches that employ a limited number of geological scenarios—typically between 10 and 20 static realizations—offer an insufficient statistical basis to capture the virtually infinite range of possible grade distributions within actual ore deposits. This limitation results in overly simplified representations of uncertainty and weakens the reliability of risk assessments. As the mining sector advances toward digital transformation and deeper integration of artificial intelligence, it becomes increasingly essential to adopt advanced optimization frameworks that harness machine learning for geological modeling, ensuring both computational efficiency and responsiveness to dynamic, evolving conditions.

Multi-agent scheduling has been applied widely in optimisation problems. Zhang et al. (2022) presents a multi-agent scheduling framework that integrates Deep Reinforcement Learning (DRL) with Proximal Policy Optimization (PPO) to handle dynamic and uncertain manufacturing environments. Experiments shows that the proposed PPO-based system outperforms traditional genetic programming and DQN approaches in convergence speed, workload balance, and scheduling efficiency for flexible job-shop operations. Recent advances in deep learning, particularly Variational Autoencoders (VAEs), offer transformative potential for geological uncertainty modelling by learning complex spatial patterns in geological data and generating realistic scenario sets that preserve geological continuity and spatial correlations. Combined with Graphics Processing Unit (GPU)-accelerated computing, these AI-enhanced approaches can address the fundamental limitations of static scenario-based planning while maintaining real-time computational performance. Barkalov&Lebedev (2017) proposed a nested optimization approach for solving multidimensional global optimization problems using both CPU and GPU resources. A complex serial algorithm runs on the CPU for global control, while a simple parallel algorithm executes on the GPU for local search. Implemented in the ExaMin solver, this hybrid scheme achieves significant computational speedup and efficiency in benchmark tests. GPU-accelerated optimization has gained momentum across various domains, from mining optimization to medical applications such as federated learning frameworks for disease detection (Mukhopadhyay et al., 2025), though application to AI-enhanced geological modeling in constrained mine scheduling remains underexplored. With the capability to execute thousands of threads in parallel, GPUs significantly reduce evaluation time for large datasets and complex AI models, making real-time geological scenario generation and near-real-time planning feasible. When integrated with hybrid metaheuristic approaches combining Genetic Algorithms (GA), Large Neighborhood Search (LNS), and Simulated Annealing (SA), GPU-based evaluation can support rapid convergence to high-quality solutions while processing dynamically generated geological scenarios, even in the presence of noisy or incomplete data.

Existing mine planning frameworks lack integrated approaches that simultaneously handle (1) AI-driven geological scenario generation with spatial correlation preservation, (2) dynamic temporal uncertainty modelling with geological realism constraints, (3) GPU-accelerated large-scale optimization with variable scenario counts, (4) real-time operational mode selection under enhanced uncertainty quantification, and (5) adaptive constraint handling through epsilon-relaxation mechanisms. Current literature addresses these challenges in isolation but not as an integrated AI-enhanced system capable of industrial-scale application with geological validity. The current work extends the work of (Rahimi I., 2025), part I, an advanced decision support system (DSS) for long-term open-pit mine planning. This study contributes to the growing body of knowledge in computational mine planning by proposing an AI-enhanced DSS that synergizes deep learning geological modeling with GPU-parallelized optimization through five novel methodological advances with clear physical interpretations.

First, VAE-based geological scenario generation learns spatial patterns from existing geological data to create realistic geological realizations that preserve spatial correlations and geological continuity, replacing static scenario sets with dynamic, geologically-consistent uncertainty representation. Second, enhanced spatial uncertainty propagation

incorporates geological proximity and spatial autocorrelation through Moran's I statistics and variogram analysis into uncertainty quantification, replacing oversimplified multiplicative factors with spatially-aware uncertainty modeling that reflects geological reality where confidence degrades with distance from drill holes and geological complexity. Third, enhanced Dantzig-Wolfe decomposition with dynamic column generation treats complete mining sequences as columns rather than individual block assignments, enabling VAE-conditioned pricing subproblems that generate mining sequences robust across dynamically sampled geological scenarios. Fourth, hybrid GA+LNS+SA metaheuristic framework with epsilon-constraint handling integrates population-based exploration through genetic algorithms, neighbourhood-based intensification through large neighbourhood search, and probabilistic acceptance through simulated annealing, while employing adaptive constraint relaxation ($\epsilon(t) = \epsilon_0 \times (1 - t/T_{\max})$) that enables broader exploration during early search phases and converges to strict feasibility requirements. Fifth, multi-agent reinforcement learning framework coordinates three specialized agents—Parameter Agent for adaptive algorithmic tuning, scheduling agent for real-time operational decisions, and resource agent for dynamic capacity allocation—with reward functions balancing NPV improvement, constraint satisfaction, computational efficiency, and risk penalty to achieve adaptive optimization throughout the planning process.

The GPU-accelerated parallel processing architecture enables real-time assessment of variable scenario counts (50-200+ scenarios) through hierarchical CUDA-based evaluation with 256 threads per block evaluating up to 262,144 candidate mining decisions simultaneously, dramatically expanding uncertainty representation while maintaining computational efficiency. Integrated operational mode selection synthesizes strategic mine planning with real-time operational mode switching under enhanced geological uncertainty, reflecting actual metallurgical plant operations where processing configurations must adapt to varying ore characteristics and recovery optimization based on improved geological understanding.

The rest of the paper is organized as follows. Section 2 shows motivation of the study. Section 3 presents the related works. Section 4 presents research methodology. Section 5 presents the problem formulation. Section 6 illustrates the proposed DSS for the case study. Section 7 depicts the Results and Numerical Study. Section 8 provides discussion. The final section delivers the conclusion and future works.

2. Motivation

The DSS presented in (Rahimi, 2025) demonstrated significant computational improvements through GPU-accelerated optimization, achieving 29.6% average speedup while maintaining robust economic performance with mean NPV of \$1.514 billion across geological scenarios. However, this framework exposed critical limitations in geological uncertainty representation that compromise the reliability of billion-dollar mining investment decisions and restrict the system's applicability across diverse geological settings. The limitations are as follows:

2.1 Limitations of Static Geological Scenario Approaches

The previous implementation proposed in the work of (Rahimi, 2025) relied on a limited set of static geological scenarios derived from the Quelopana & Navarra (2024) dataset, which provides insufficient statistical foundation for comprehensive uncertainty quantification in large-scale mining operations. This fixed scenario approach suffers from several fundamental weaknesses: (1) the narrow NPV range (\$1.485-\$1.543 billion) with only \$58 million spread across scenarios may indicate artificially constrained uncertainty rather than comprehensive risk assessment, (2) static scenario sets (typically 10-20 realizations) cannot adapt to new geological information or explore the full spectrum of geological uncertainty inherent in complex deposits, and (3) fixed scenario probabilities throughout the planning horizon fail to incorporate information updates from ongoing mining operations and evolving geological understanding.

2.2 Theoretical Weaknesses in Uncertainty Modelling

The multiplicative uncertainty formulation ($\sigma_{\{s,t\}} = \gamma_s \times \phi_t$) employed in the previous work (Rahimi, 2025) represents a significant theoretical limitation that undermines geological realism. One of the main limitation of the approach assumes independence between spatial and temporal uncertainty components, failing to capture the fundamental geological principle that uncertainty varies spatially based on data density, geological complexity, and proximity to drill holes. The static scenario-specific weights (γ_s) cannot adapt to evolving geological understanding, while the uniform temporal decay assumption (ϕ_t) oversimplifies how geological knowledge actually deteriorates across varying geological domains and planning horizons.

2.3 Validation Scope Limitations

The previous validation framework was restricted to a single gold-copper porphyry deposit type, providing no evidence of performance across the diverse geological settings where mining operations occur. The geological feature set lacked essential attributes including alteration intensity, structural geology, and mineralization styles that significantly influence both grade continuity and operational constraints. The absence of spatial correlation modelling means the system cannot properly represent geological continuity, potentially generating operationally infeasible mining sequences that violate fundamental geological principles.

2.4 Industry Need for AI-Enhanced Geological Modelling

The above-mentioned limitations (2.1-2.3) create a compelling research gap that justifies developing an AI-enhanced geological modelling framework integrated with proven GPU optimization architecture. The mining industry urgently needs DSS that can: (1) generate realistic geological scenarios dynamically using deep learning approaches that preserve spatial correlations and geological continuity, (2) incorporate enhanced spatial uncertainty propagation that reflects actual geological complexity rather than oversimplified multiplicative factors, (3) adapt to new geological data in real-time through machine learning approaches, and (4) provide comprehensive validation across diverse deposit types and geological settings.

2.5 Column Generation Inefficiency

The implemented Dantzig-Wolf decomposition in the work of (Rahimi, 2025) generates columns independently for each equipment unit without considering geological correlation between adjacent blocks, leading to suboptimal mining sequences that violate geological continuity principles. Also, the current work integrated approaches that simultaneously handle spatially-aware column generation where mining sequences respect geological

boundaries along with VAE-conditioned scenario generation within the pricing subproblem and GPU-accelerated spatial constraint propagation during route construction.

2.6 Population Diversity and Solution Space Exploration Deficiencies

The LNS+SA hybrid approach in (Rahimi, 2025), while achieving 29.6% computational speedup, exhibits fundamental limitations in solution space exploration that compromise its ability to identify globally optimal mining sequences under geological uncertainty. The framework's reliance on sequential neighborhood destruction-repair cycles restricts exploration to solution trajectories defined by iterative perturbations from a single solution, creating path dependency that may miss superior mining sequences in distant regions of the solution space. This limitation becomes particularly critical in large-scale mine planning where the combinatorial explosion of feasible schedules (with 50,000 blocks across 6 periods yielding approximately $10^{50,000}$ possible sequences) requires systematic exploration mechanisms beyond local neighborhood search.

Current metaheuristic approaches in mining optimization exhibit specific weaknesses that genetic algorithms address: (1) Premature convergence in SA-based methods. Danish et al. (2021) and Kumral & Dowd (2005) demonstrate that SA alone converges to local optima when geological heterogeneity creates multi-modal objective landscapes with numerous sub-optimal plateaus, (2) Limited diversity maintenance in LNS. Blom et al. (2024) shows that destruction-repair cycles, while effective for constraint satisfaction, do not maintain solution diversity necessary for exploring fundamentally different extraction strategies, and (3) Lack of crossover-based recombination - existing approaches miss the opportunity to combine favorable mining sequence characteristics from multiple high-quality solutions, a capability demonstrated by Muke et al. (2025) and Navarro et al. (2024) where GA crossover operators successfully merge complementary extraction patterns.

The mining optimization literature provides compelling evidence for GA integration. Muke et al. (2025) demonstrated that genetic algorithms excel at aligning temporal and spatial scheduling constraints through population-based exploration, achieving solutions that coordinate long-term strategic planning with medium-term operational requirements. Navarro et al. (2024) showed that parallel genetic algorithms successfully handle geometrically constrained production scheduling, though their reliance on best-case scheduling proxies and sensitivity to geometric parameters indicates the need for hybrid approaches. These works collectively suggest that GA's population-based search, when combined with local refinement mechanisms (LNS) and acceptance criteria (SA), can overcome the individual limitations of each metaheuristic while preserving their respective strengths.

3. Related Works

Current mine planning research places growing emphasis on how uncertainty influences extraction and processing decisions. Geological uncertainty poses particularly significant challenges, since errors in estimating ore grades or incorrectly characterizing rock properties can result in inefficient extraction sequences and reduced profitability (Rimélé et al, 2020). Conventional methodologies have been largely deterministic, failing to adequately account for uncertainty within their modeling frameworks (Hustrulid et al., 2013; Osanloo et al., 2008; Boland et al., 2009; Ramazan, 2007).

To address these challenges, researchers have developed scenario-based and stochastic modelling approaches that evaluate multiple possible outcomes of uncertain parameters (Upadhyay & Askar-Nasab, 2018; MacNeil & Dimitrakopoulos, 2017). Cutler & Dimitrakopoulos (2024) presented a two-stage stochastic integer programming framework that simultaneously optimizes long-term pit scheduling and access infrastructure design, incorporating accessibility requirements through checkpoints, ramps, and bench roads; application to a gold deposit demonstrated integrated ramp network design while maintaining ore grade targets. Muke et al., (2025) developed a mixed-integer programming formulation coupled with genetic algorithm optimization to bridge long-term and medium-term scheduling horizons in open-pit operations, achieving grade-tonnage alignment and ensuring temporal-spatial consistency via penalty function mechanisms. Chen et al. (2025) tackled production planning under combined geological and economic uncertainty through Monte Carlo simulation of grade and cost distributions, employing NSGA-II multi-objective optimization with weighted grey relational analysis; a commodity price sensitivity module triggers iterative plan adjustments responsive to market fluctuations, followed by Pareto-optimal solution ranking. Jiang & Dimitrakopoulos (2024) augmented this methodology by integrating stochastic equipment capacity modeling and constraint penalty mechanisms within the two-stage optimization structure, generating capacity-feasible mine-life schedules that achieved approximately 2% NPV improvement in a copper mining complex application.

Nevertheless, these approaches frequently encounter limitations in scalability and computational efficiency, particularly when addressing extensive mining operations involving thousands of extraction blocks across multiple decades of planning horizons. The increasing sophistication of such optimization frameworks has driven the integration of high-performance computing infrastructure and novel algorithmic strategies, encompassing metaheuristic approaches, hybrid optimization techniques, and parallel processing architectures.

Also, researchers frequently employ decomposition methods in open-pit mining optimization, though challenges remain (Blom et al., 2016; Fathollahzadeh et al., 2021). A significant advancement involves applying decomposition techniques, especially Dantzig-Wolfe decomposition, which partitions large-scale mine planning challenges into smaller, more manageable subproblems. This hierarchical optimization framework facilitates more precise decision-making across both strategic and tactical planning levels. The master problem coordinates the overall extraction timeline, while subproblems assess specific mining configurations across different operational modes and uncertainty scenarios. Beyond improving computational performance, this decomposition approach offers enhanced capability for modeling the complex relationships among extraction blocks, equipment limitations, and processing plant capacity constraints.

Beyond implementing sophisticated optimization techniques, contemporary mine planning systems must contend with the substantial computational demands of assessing numerous potential extraction scenarios. This issue becomes especially pronounced in stochastic and robust optimization contexts, which require the simultaneous analysis of multiple geological realizations. Over recent decades, open-pit mine production scheduling (OPMPS) has received considerable research attention given its fundamental importance to mining operation profitability. Early methodologies employed linear programming approaches, exemplified by

Johnson's (1969) pioneering work that utilized Dantzig-Wolfe decomposition combined with network flow algorithms.

Several researchers explored alternative mathematical programming techniques for mine scheduling optimization. Dagdelen (1986) employed integer programming combined with Lagrangian relaxation methods, while Caccetta and Hill (2003) implemented branch-and-cut algorithms suitable for moderately-sized mining operations. Dynamic programming methodologies were investigated by Elevli (1995) and Erarslan & Çelebi (2001), although these approaches demonstrated limited applicability to larger-scale operations. Mixed-Integer Programming (MIP) formulations were introduced by Gershon (1983) and subsequent researchers, yet these techniques frequently encounter computational tractability issues when applied to industrial-scale mining problems. Researchers have pursued various strategies to mitigate computational burden, including block aggregation methodologies (Ramazan et al., 2005) and sophisticated decomposition algorithms incorporating cutting plane techniques (Bley et al., 2010; Askari-Nasab et al., 2011; Lambert & Newman, 2014). Notwithstanding these advances, the majority of existing methodologies remain constrained to simplified problem formulations or small-to-medium scale applications, primarily due to the inherent combinatorial complexity of open-pit mine production scheduling and the exponential growth of constraints and decision variables in realistic problem instances.

In response to computational limitations, the mining research community has progressively adopted heuristic and metaheuristic optimization strategies for open-pit mine production scheduling. Various nature-inspired and evolutionary computation methods have demonstrated capability in producing near-optimal solutions for complex, large-scale scheduling challenges, including genetic algorithms (Denby & Schofield, 1994; Alipour et al., 2019), Tabu Search coupled with Variable Neighborhood Descent (Lamghari & Dimitrakopoulos, 2012), Ant colony optimization (Soleymani Shishvan & Sattarvand, 2015), Particle Swarm Optimization (Khan & Niemann-Delius, 2014, 2018; Khan, 2018), and Differential Evolution approaches. Navarro et al. (2024) developed a parallelized genetic algorithm addressing geometrically constrained scheduling challenges, wherein solution representations consist of centroid configurations (genotype) transformed via MeanShift clustering into truncated-cone extraction phases (phenotype), with fitness evaluation performed through rapid best-case sequential scheduling heuristics approximating NPV under operational constraints. However, this approach exhibits limitations including reliance on non-operational scheduling proxies for fitness assessment, sensitivity to geometric parameterization, and potential failure to identify globally optimal solutions.

Probabilistic optimization frameworks, exemplified by research from Dimitrakopoulos & Senécal (2019) and Montiel & Dimitrakopoulos (2013), have been deployed to manage geological uncertainty and accommodate multiple mineral processing pathways. Laloy et al. (2017) introduces a deep variational autoencoder (VAE) framework to perform low-dimensional parameterization of complex geological media for inversion problems. Liu et al. (2022) examined uncertainty quantification in geophysical inverse problems using Variational Autoencoders (VAEs) for dimensionality reduction combined with MCMC and ES-MDA methods. VAEs enable efficient inversion by learning nonlinear probability distributions in low-dimensional spaces, making computationally intensive problems tractable while capturing complex spatial patterns better than linear methods. Liu et al. (2022) find model reduction

underestimates uncertainty while data reduction overestimates it, though VAE-based data reduction effectively mitigates ensemble collapse in ES-MDA applications. By training the VAE on thousands of multiple-point statistics (MPS) realizations, the authors achieve efficient and realistic sampling of geological structures while maintaining geological consistency. Mosser L., et al (2020) presents a novel Bayesian inversion framework that combines Generative Adversarial Networks (GANs) with the acoustic wave equation to reconstruct subsurface geological structures. The GAN acts as a geological prior, generating realistic geological heterogeneities from a low-dimensional latent space, while the adjoint-state method computes gradients for efficient inversion. Dupont et al. (2018) introduced a GAN-based semantic inpainting approach to generate geological realizations that both honor sparse physical measurements and reproduce realistic subsurface patterns. By training a DC-GAN on fluvial geological images generated from object-based models, the method learns a distribution of geological structures and uses context and prior losses to constrain outputs to known data points. Canchumuni et al. (2021) introduced a framework combining deep generative models (VAEs, GANs, Cycle-GANs) with the Ensemble Smoother (ES-MDA) to achieve geologically realistic facies history matching. It maps complex geological structures into a continuous latent space, enabling efficient and consistent data assimilation. Results showed VAEs and Cycle-GANs outperform others by preserving geological realism, uncertainty, and computational efficiency.

Additionally, hybrid methodologies integrating Lagrangian Relaxation with bio-inspired algorithms such as Firefly and Bat optimization (Tolouei et al., 2020a, 2020b, 2020c) have emerged to enhance solution quality under uncertain conditions. Simulated Annealing techniques (Kumral & Dowd, 2005; Kumral, 2013) have found application across diverse scheduling contexts, including ore-waste classification and stochastic long-term planning, with computational efficiency improvements achieved through memory-enhanced variants (Sari & Kumral, 2016). Notwithstanding these methodological advances, stockpiling considerations remain inadequately addressed within most contemporary OPMPs frameworks, underscoring the necessity for more comprehensive modeling approaches capable of capturing such operational complexities.

Blom and colleagues (2024) introduced a LNS methodology for addressing large-scale open-pit mine scheduling challenges. Their approach begins with a feasible baseline schedule created through a sliding window heuristic, then progressively refines it by solving restricted mixed-integer programming subproblems that modify only specific decision variables at each iteration. By leveraging the inherent structure of mine planning problems to construct effective search neighborhoods, their method can handle mine models of realistic scale that exceed the computational capacity of commercial optimization solvers. The authors validated their approach through two real-world applications: Mongolia's Oyu Tolgoi copper-gold operation and Western Australia's Pilbara iron ore complex. These case studies demonstrated the method's capability to generate near-optimal mining schedules with substantial computational time savings compared to traditional approaches. For major mining companies such as Rio Tinto, this technique facilitates the rapid development of high-quality mine plans and enables comprehensive evaluation of alternative production strategies, ultimately supporting more informed long-term operational decision-making.

Danish, A. A., et al., (2021) proposed a SA-based optimisation approach for long-term open-pit mine production scheduling, integrating a stockpiling option to handle nonlinear constraints

related to grade mixing. The method starts with an initial sub-optimal solution generated via a ranked positional weight heuristic, which considers block precedence and mining capacities but may violate processing constraints. A stockpile heuristic is then applied to adjust processing feasibility by storing or reclaiming ore between periods. The SA algorithm optimizes the schedule by perturbing block sequences while honoring mining, processing, and precedence constraints, with the stockpile option allowing flexible ore blending. Additionally, a Greedy Heuristic improves the SA's convergence by prioritizing high-grade block extraction in early periods. The approach was tested on three real-world mine datasets from Minelib, achieving near-optimal solutions significantly faster than traditional CPLEX optimisation, with demonstrated improvements in NPV and computational efficiency. The study concludes that combining SA with stockpiling and greedy heuristics effectively solves large-scale, complex open-pit production scheduling problems. Das et al. (2024) develop a MILP that simultaneously schedules ore extraction and waste dumping (incl. in-pit) while choosing shortest-path haul roads from a Dijkstra-generated database. In the above-mentioned work, they pair this with weighted topological sort and simulated annealing to scale up; in a real case it cut average haul distances by ~39% and increased in-pit backfilling by ~44% versus planning software.

The proposed advancement beyond prior frameworks lies in three specific areas: Blom et al. (2024) focuses on CPU-based LNS without uncertainty modelling or operational mode integration; Danish et al. (2021) addresses stockpiling in SA but lacks GPU acceleration and dynamic uncertainty; our framework uniquely combines GPU-parallelized evaluation with time-dependent uncertainty factors and integrated operational mode selection, enabling real-time scenario analysis for 50,000 block problems that exceed the capabilities demonstrated in prior works.

The proposed methodological contributions extend in three specific conceptual advances: (1) dynamic uncertainty evolution framework introducing time-dependent uncertainty factors that explicitly capture geological confidence degradation over planning horizons, contrasting with static uncertainty approaches in Blom et al. (2024) and Danish et al. (2021) that treat uncertainty as time-invariant, (2) hierarchical GPU-Accelerated constraint repair methodology developing novel multi-level parallel repair mechanisms that transform traditional sequential constraint handling into massively parallel feasibility restoration enabling concurrent evaluation of 262,144 candidate moves, and (3) Uncertainty-Adaptive column generation extending Dantzig-Wolfe decomposition with dynamic scenario evaluation where column generation continuously adapts based on evolving uncertainty realizations rather than static decomposition approaches. These methodological innovations create new theoretical capabilities for temporal uncertainty propagation in mining optimization, parallel constraint repair at industrial scale, and adaptive decomposition under dynamic uncertainty—representing conceptual advances beyond algorithmic integration. The framework enables previously impossible computational scenarios for uncertainty-aware mine planning by combining these methodological concepts within a unified optimization architecture. This represents fundamental advancement in mining optimization methodology rather than purely engineering application of existing techniques.

4. Research Methodology

This research employs a comprehensive four-phase methodology designed to address the limitations identified in the work of (Rahimi I., 2025) while integrating advanced artificial intelligence techniques for enhanced geological uncertainty modelling and optimization performance. The methodology systematically progresses from foundational AI enhancements through scalability assessment to rigorous benchmarking and validation, ensuring scientific rigor and practical applicability. The research methodology has been conducted in several phases as follows:

4.1 VAE-Based Geological Scenario Generation

The first major enhancement replaces the static scenario limitation of the work of (Rahimi I., 2025) with a dynamic VAE framework for geological modelling. The VAE architecture consists of an encoder network that maps input geological data (grade distribution, rock types, spatial coordinates, and enhanced geological features) to probability distributions in latent space, and a decoder network that generates realistic geological scenarios from sampled latent vectors. The VAE training objective combines reconstruction accuracy with geological realism through a custom loss function:

$$L_VAE = L_reconstruction + \beta \cdot L_KL + \lambda \cdot L_geological \quad (1)$$

where $L_reconstruction$ measures geological scenario reconstruction quality, L_KL ensures proper latent space distribution, and $L_geological$ enforces geological constraints such as spatial continuity and grade-tonnage relationships.

4.2 Improved Dantzig-Wolfe Decomposition

The proposed Dantzig-Wolfe implementation in the work of (Rahimi, 2025) treats individual block-period assignments as decision variables. A significant enhancement would restructure this into complete mining sequences as columns. Instead of generating columns for single block assignments, the enhanced framework would generate complete extraction sequences spanning multiple periods and geological scenarios.

Each column would represent a feasible mining sequence: a temporally and spatially consistent path through the block model that respects precedence constraints while adapting to geological uncertainty. The master problem would then select the optimal combination of these sequences to maximize overall NPV while satisfying capacity and operational constraints.

4.2.1 Dynamic VAE-Integrated Pricing

Within the enhanced pricing subproblem, geological scenarios would no longer be static inputs but dynamically generated using proposed VAE framework. During each column

generation iteration, the pricing algorithm would sample new geological realizations from the trained VAE, creating mining sequences that are robust across this expanded uncertainty space.

The pricing subproblem would solve: given current dual prices from the master problem, generate the mining sequence with the most negative reduced cost across dynamically sampled geological scenarios. This requires solving small optimization problems during sequence generation. In this context, this means optimizing operational mode selection and spatial uncertainty factors as mining sequences are built, rather than treating these as fixed parameters.

The enhanced spatial uncertainty propagation could be integrated directly into the column generation process. Rather than applying uncertainty factors uniformly, the column pool would dynamically adapt based on spatial correlation patterns learned during the optimization process. As new geological information becomes available through the VAE or actual mining operations, the column generation would re-evaluate existing sequences and generate new ones that better reflect updated uncertainty distributions.

The framework would maintain a dynamic column pool where older columns representing outdated geological understanding are periodically removed, while new columns incorporating improved spatial uncertainty modeling are continuously added. This creates an adaptive optimization process that learns and improves geological representation throughout the solution process, addressing limitation of static scenario-based uncertainty modelling proposed in the work of (Rahimi, 2025). The key features of the enhanced Dantzig-Wolfe Decomposition is as follows:

Phase 1: AI-Enhanced Initialization The VAE geological scenario generator creates the probabilistic foundation by learning spatial patterns from historical geological data. The enhanced spatial uncertainty propagation ($\sigma_{\text{enhanced}}(s,t) = f_{\text{spatial}} \times \phi_{\text{temporal}} \times \psi_{\text{geological}}$) replaces static multiplicative factors introduced by (Rahimi, 2025) with spatially-aware modeling. The reinforcement learning agents (Parameter, Scheduling, and Resource agents) are initialized to adapt the optimization parameters based on geological complexity and operational constraints.

Phase 2: Dynamic Scenario-Aware Column Generation During each iteration, the VAE generates new geological realizations conditioned on current dual information, enabling the system to explore geological uncertainty spaces that become economically attractive as dual values evolve. The spatial uncertainty factors are dynamically updated using Moran's I spatial autocorrelation and geological features. Most importantly, mining sequences are constructed as complete extraction paths for equipment units, where each column represents not just a block-period assignment but a full operational strategy including operational mode switching guided by the reinforcement learning framework.

Phase 3: Intelligent Column Pool Management The multi-agent reinforcement learning system enables adaptive learning where geological understanding evolves throughout optimization. The Parameter Agent adjusts SA/LNS parameters based on convergence patterns, the Scheduling Agent optimizes operational decisions using the reward function $R(t) =$

$\alpha \cdot \text{NPV_improvement} + \beta \cdot \text{Constraint_satisfaction} + \gamma \cdot \text{Computational_efficiency} - \delta \cdot \text{Risk_penalty}$, and the Resource Agent manages dynamic capacity allocation as geological scenarios change. The methodology has been presented in Algorithm 1.

Algorithm 1 Enhanced Dantzig–Wolfe with VAE and Multi-Agent RL

- 1: **Input:** Block model \mathcal{B} , geological data \mathcal{G} , planning periods T
- 2: **Output:** Optimal mining schedule \mathcal{S}^*
- 3: **Phase 1: AI-Enhanced Initialization**
- 4: Initialize VAE($\theta_{\text{enc}}, \theta_{\text{dec}}$) with geological constraints $L_{\text{geological}}$
- 5: Train VAE on historical data: $\min L_{\text{recon}} + \beta L_{\text{KL}} + \lambda L_{\text{geological}}$
- 6: Initialize RL agents: **Agent_param**, **Agent_schedule**, **Agent_resource**
- 7: Compute initial spatial uncertainty: $\sigma_{\text{enhanced}}(s, t) = f_{\text{spatial}} \times \phi_{\text{temporal}} \times \psi_{\text{geological}}$
- 8: Generate initial column set \mathcal{C}^0 using greedy heuristic
- 9: $k \leftarrow 0$, $\text{dual}^0 \leftarrow \mathbf{0}$
- 10: **repeat**
- 11: **Phase 2: Dynamic Column Generation**
- 12: **Master Problem:** Solve LP relaxation
- 13: $\text{dual}^{k+1} \leftarrow$ extract duals ($\pi^f, \pi^{\text{capacity}}, \pi^{\text{precedence}}$)
- 14: **VAE Scenario Generation:**
- 15: Sample $z \sim \mathcal{N}(\mu, \sigma^2)$ conditioned on dual^{k+1}
- 16: $\mathcal{S}_{\text{new}} \leftarrow \text{VAE}_{\text{decoder}}(z; \theta_{\text{dec}})$
- 17: $\mathcal{S}_{\text{valid}} \leftarrow \{s \in \mathcal{S}_{\text{new}} : L_{\text{geological}}(s) < \tau\}$
- 18: **Spatial Uncertainty Update:**
- 19:
$$I_{\text{Moran}} = \frac{N \sum_{i,j} w_{ij} (x_i - \bar{x})(x_j - \bar{x})}{\sum_{i,j} w_{ij} \sum_i (x_i - \bar{x})^2}$$
- 20: $\sigma_{\text{enhanced}}^{k+1}(s, t) = (1 - I_{\text{Moran}} + \sigma_{\text{local}}) \times \phi_{\text{temporal}}(t) \times \psi_{\text{geological}}$
- 21: **RL-Guided Subproblem Solving:**
- 22: **for** each equipment type $e \in \mathcal{E}$ **do**
- 23: **Agent_schedule** selects subproblem strategy based on dual^{k+1}
- 24: Solve pricing subproblem with enhanced uncertainty:
- 25: $\min \sum_{b,t} (c_{bt} - \pi_{bt}^f) x_{bt} + \sum_{s \in \mathcal{S}_{\text{valid}}} \sigma_{\text{enhanced}}^{k+1}(s, t) \cdot \text{ENPV}_{bt}^s$
- 26: Subject to: precedence, capacity, operational-mode constraints
- 27: Generate mining-sequence column col_{new} (GPU-accelerated)
- 28: **if** reduced cost of $\text{col}_{\text{new}} < 0$ **then**
- 29: $\mathcal{C}^{k+1} \leftarrow \mathcal{C}^k \cup \{\text{col}_{\text{new}}\}$
- 30: **end if**
- 31: **end for**
- 32: **Phase 3: Adaptive Column Pool Management**
- 33: $\text{quality} = \alpha \cdot \text{NPV}_{\text{impr}} + \beta \cdot \text{geological_consistency} - \gamma \cdot \text{computational_cost}$
- 34: $\mathcal{C}^{k+1} \leftarrow \{\text{col} \in \mathcal{C}^{k+1} : \text{quality}(\text{col}) > \tau_{\text{min}}\}$
- 35: **RL Learning Update:**
- 36: $R^{k+1} = \alpha \cdot \Delta \text{NPV} + \beta \cdot \text{constraint_satisfaction} + \gamma \cdot \text{efficiency} - \delta \cdot \text{risk}$
- 37: $\theta_{\text{agent}}^{k+1} \leftarrow \theta_{\text{agent}}^k + \alpha_{\text{RL}} \nabla_{\theta} J(\theta_{\text{agent}}^k)$
- 38: **Agent_param** adjusts SA/LNS parameters based on convergence rate
- 39: $k \leftarrow k + 1$
- 40: **until** no columns with negative reduced cost are found **or** max iterations reached
- 41: **Final Solution:**
- 42: Solve integer master problem with final column set $\mathcal{C}^{\text{final}}$
- 43: **return** Optimal mining schedule \mathcal{S}^*

4.3 Enhanced Spatial Uncertainty Propagation

The methodology introduces spatially-aware uncertainty modeling that incorporates geological proximity and spatial autocorrelation, replacing oversimplified multiplicative factors with:

$$\sigma_{\text{enhanced}}(s,t) = f_{\text{spatial}}(\text{grades, coordinates}) \times \varphi_{\text{temporal}}(t) \times \psi_{\text{geological}}(\text{features}) \quad (2)$$

The spatial component f_{spatial} captures spatial autocorrelation using Moran's I statistic and variogram analysis, while $\psi_{\text{geological}}$ incorporates enhanced geological features including alteration intensity, structural density, and distance to intrusion. This formulation addresses the theoretical weakness of assuming independence between spatial and temporal uncertainty components.

4.4 Reinforcement Learning Integration

A multi-agent reinforcement learning framework is implemented to address parameter sensitivity and enable adaptive optimization. The framework consists of three specialized agents: a Parameter Agent for adaptive SA/LNS parameter tuning, a Scheduling Agent for real-time operational decisions, and a Resource Agent for dynamic capacity allocation. The reward function balances NPV improvement, constraint satisfaction, computational efficiency, and risk penalty:

$$R(t) = \alpha \cdot \text{NPV_improvement} + \beta \cdot \text{Constraint_satisfaction} + \gamma \cdot \text{Computational_efficiency} - \delta \cdot \text{Risk_penalty} \quad (3)$$

4.5 Large Neighbourhood Search (LNS), Genetic Algorithm (GA), and Simulated Annealing (SA)

The hybrid proposed extension integrates genetic algorithm population dynamics with the established LNS+SA framework through adaptive neighborhood decomposition. The solution space is partitioned into overlapping neighborhoods based on geological similarity, spatial proximity, and temporal clustering. Each neighborhood is explored using a specialized GA variant that maintains population diversity while respecting local constraint structures.

The epsilon-constraint handling mechanism adapts mining precedence constraints during early search phases, allowing controlled exploration of near-feasible regions. The tolerance parameter $\varepsilon(t) = \varepsilon_0 \times (1 - t/T_{max})$ decreases linearly, where t represents current iteration and T_{max} is maximum iterations. This enables broader search exploration initially while converging to strict feasibility requirements. Population-based exploration occurs within each neighborhood, where genetic operators (crossover, mutation) are constrained to maintain geological realism and operational feasibility. The SA acceptance criterion governs transitions between neighborhoods, while LNS destruction/repair mechanisms handle infeasibility restoration when ε tolerance is exceeded. Algorithm 2 presents the integration of these three metaheuristics. It begins by generating an initial population of candidate schedules using a heuristic and assigns a maximum tolerance for constraint violations. The solution space is then divided into neighborhoods based on geological similarity, which helps preserve problem-specific structure during search. Iterations proceed while the maximum time limit has not been reached and convergence is not achieved.

Within each neighborhood, the algorithm updates the ε -constraint to gradually tighten feasibility conditions over time. Then, a GA-based exploration is performed: parents are selected using tournament selection, offspring are generated through geology-aware crossover, and mutations are applied while maintaining precedence relations. Fitness is evaluated using a relaxed constraint framework, where schedules are penalized based on the degree of violation relative to the current ε -threshold. This balances exploration of promising but slightly infeasible solutions with the drive toward feasibility.

For solutions that remain infeasible, the LNS module applies a targeted repair process. It destroys and reconstructs parts of the solution, focusing on violated constraints, and employs GPU acceleration to speed up the repair phase. If the modified solution improves feasibility or quality, it replaces the previous one. Next, the SA-based neighborhood transition decides whether to move from the current neighborhood to another based on solution improvement and a probabilistic acceptance criterion. This step prevents premature convergence by allowing occasional acceptance of worse solutions.

Finally, populations from all neighborhoods are merged, elitist selection ensures the best candidates survive, and strongly infeasible solutions are removed once the ε -threshold drops below a limit. The temperature parameter for SA is cooled gradually, and iterations continue. After termination, the algorithm performs a strict feasibility check with ε set to zero, applies a final LNS repair if needed, and returns the best feasible mining schedule. This hybrid framework combines global exploration, local repair, and probabilistic diversification, making it robust for handling the complex and constrained nature of open-pit mining optimization

Algorithm 2 Hybrid GA+LNS+SA with ε -Constraint Handling

```
1: Input: Block model  $\mathcal{B}$ , neighborhoods  $\mathcal{N} = \{N_1, N_2, \dots, N_k\}$ , population size  $P$ 
2: Output: Optimal mining schedule  $\mathcal{S}^*$ 
3: Initialize population  $Pop^0 = \{S_1^0, S_2^0, \dots, S_P^0\}$  using Algorithm 2 heuristic
4: Set initial  $\varepsilon$ -tolerance:  $\varepsilon^0 = \varepsilon_{\max}$ 
5: Decompose solution space into neighborhoods based on geological similarity
6:  $t \leftarrow 0, T \leftarrow T_0$ 
7: converged  $\leftarrow$  false
8: while  $t < T_{\max} \wedge \neg$ converged do
9:   for each neighborhood  $N_i \in \mathcal{N}$  do
10:     $\varepsilon$ -Constraint Update
11:     $\varepsilon^t \leftarrow \varepsilon_{\max} \left(1 - \frac{t}{T_{\max}}\right)$ 
12:    Population-Based Exploration in  $N_i$ 
13:    for gen = 1 to  $G_{\max}$  do
14:      Select parents using tournament selection from  $Pop^t$ 
15:      offspring  $\leftarrow$  CROSSOVER(parent1, parent2,  $N_i$ )
16:      Apply spatial mutation with precedence preservation
17:      Evaluate fitness with  $\varepsilon$ -relaxed constraints:
18:       $fitness(S) \leftarrow NPV(S) - penalty \cdot \max(0, violation(S) - \varepsilon^t)$ 
19:    end for
20:    LNS Repair for Infeasible Solutions
21:    for each solution  $S \in Pop^t$  with  $violation(S) > \varepsilon^t$  do
22:      Apply destruction phase targeting violated constraints
23:      Perform GPU-accelerated repair (Algorithm 3)
24:      Update solution if improvement found
25:    end for
26:    SA-Based Neighborhood Transition
27:    Evaluate best solution  $S_{best}^{N_i}$  in current neighborhood
28:    if  $f(S_{best}^{N_i}) > f(S_{current}) + \text{random}() \cdot T$  then
29:      Accept transition to  $N_{i+1}$ 
30:       $S_{current} \leftarrow S_{best}^{N_i}$ 
31:    end if
32:  end for
33:  Population Update
34:  Combine populations from all neighborhoods
35:  Apply elitist selection to maintain population size  $P$ 
36:  if  $\varepsilon^t < \varepsilon_{\text{threshold}}$  then remove solutions with  $violation(S) > \varepsilon^t$ 
37:   $T \leftarrow T \cdot \alpha$ 
38:   $t \leftarrow t + 1$ 
39: end while
40: Final Feasibility Check
41: Apply strict constraint validation with  $\varepsilon = 0$ 
42: Perform final LNS repair if necessary
43: return Best feasible solution  $\mathcal{S}^*$ 
```

The Figure 1 (a-b) visualization illustrates the fundamental exploration-exploitation balance mechanism in the hybrid GA+LNS+SA metaheuristic for open-pit mine scheduling optimization. The figure demonstrates how the algorithm systematically transitions from broad search space exploration to focused solution refinement across two representative iterations. In the exploration phase (Iteration 1), genetic algorithm population diversity and large neighborhood search destruction create substantial solution variability, while high epsilon-constraint tolerance ($\varepsilon(t) = \varepsilon_0 \times (1 - t/T_{\max})$) permits exploration of near-feasible regions. The exploitation phase (Iteration 2) emphasizes local intensification through targeted LNS repair operations and simulated annealing acceptance criteria, while progressively tightening constraint tolerance guides convergence toward strictly feasible, high-quality mining schedules. The color-coded blocks represent different mining periods (1-6) and destroyed blocks (gray), visually demonstrating how the hybrid approach balances global exploration with local refinement while maintaining operational feasibility through adaptive constraint handling mechanisms.

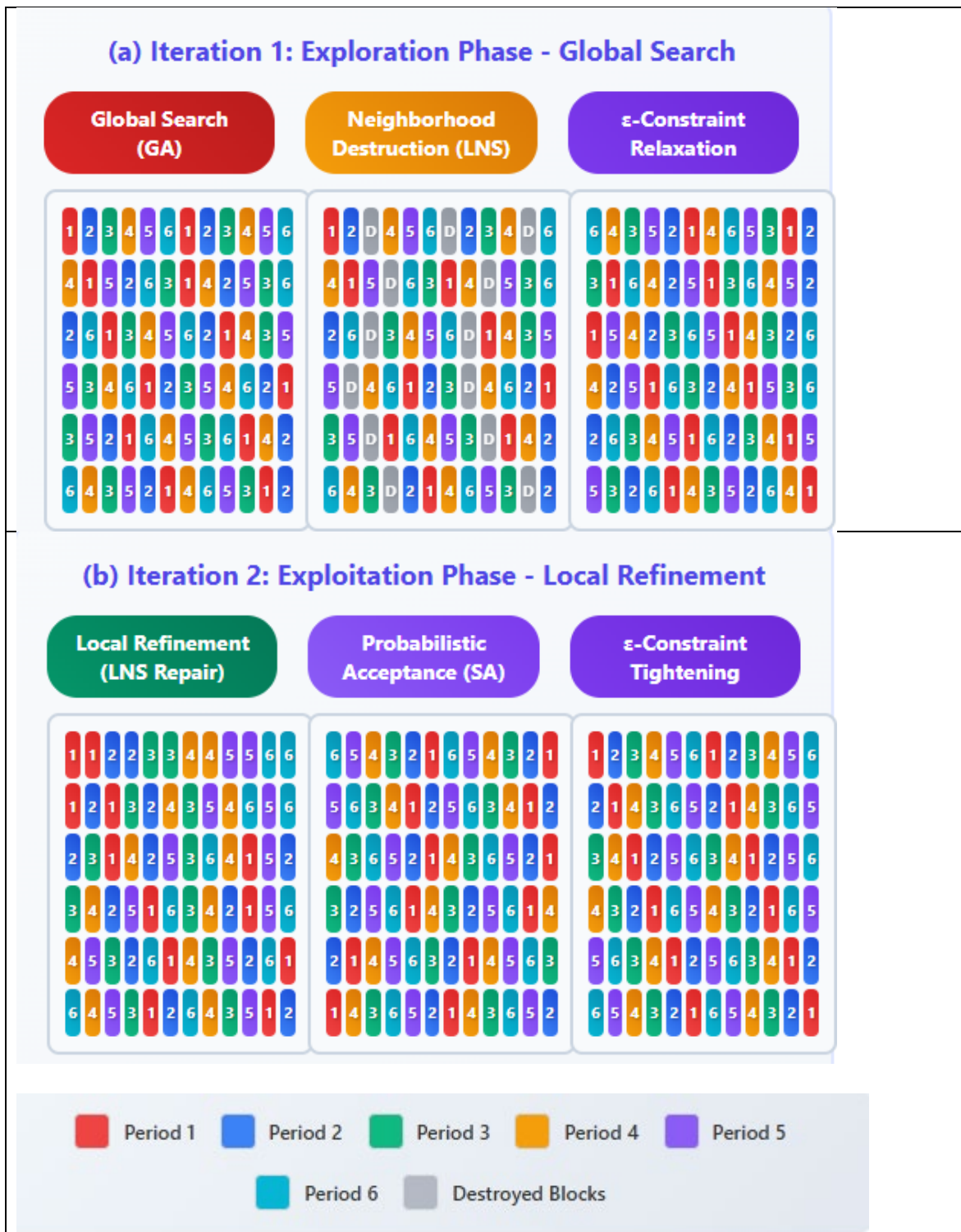


Figure 2 presents the technology stack & infrastructure for the proposed DSS. The proposed AI-enhanced mining DSS employs a comprehensive technology stack designed to ensure scalability, reproducibility, and seamless integration across diverse computational environments. The infrastructure architecture is built upon a container-based deployment strategy that addresses the critical requirements for both research reproducibility and industrial deployment scalability. The system utilizes Docker containerization to encapsulate the entire computational environment, ensuring consistent behavior across development, testing, and production environments. This approach eliminates the "it works on my machine" problem commonly encountered in complex optimization systems that integrate multiple computational paradigms. Kubernetes orchestration provides automated scaling capabilities, enabling the DSS to dynamically allocate computational resources based on problem complexity and available infrastructure. This container-first approach directly addresses reviewer concerns regarding deployment consistency and enables seamless migration between local development environments, high-performance computing clusters, and cloud platforms. The technology stack integrates state-of-the-art frameworks across multiple computational domains. Deep learning components leverage PyTorch and TensorFlow for VAE implementation, providing the flexibility needed for custom geological constraint integration within the neural network architecture. Reinforcement learning capabilities are implemented through Stable-Baselines3 and Ray RLLib, enabling distributed training of multi-agent systems for adaptive parameter optimization. The GPU computing layer utilizes CUDA 12.0+ with cuDNN optimizations, while NVIDIA Nsight provides comprehensive profiling capabilities to address previous limitations in performance analysis. To address benchmarking limitations identified in previous work (Rahimi, 2025), the infrastructure incorporates direct interfaces to commercial solvers through CPLEX API. This integration enables systematic performance comparison under controlled conditions, addressing the critical gap in commercial solver benchmarking. The monitoring infrastructure, built on Prometheus and Grafana, provides real-time performance tracking and automated alerting for performance degradation, ensuring system reliability during extensive benchmarking campaigns.

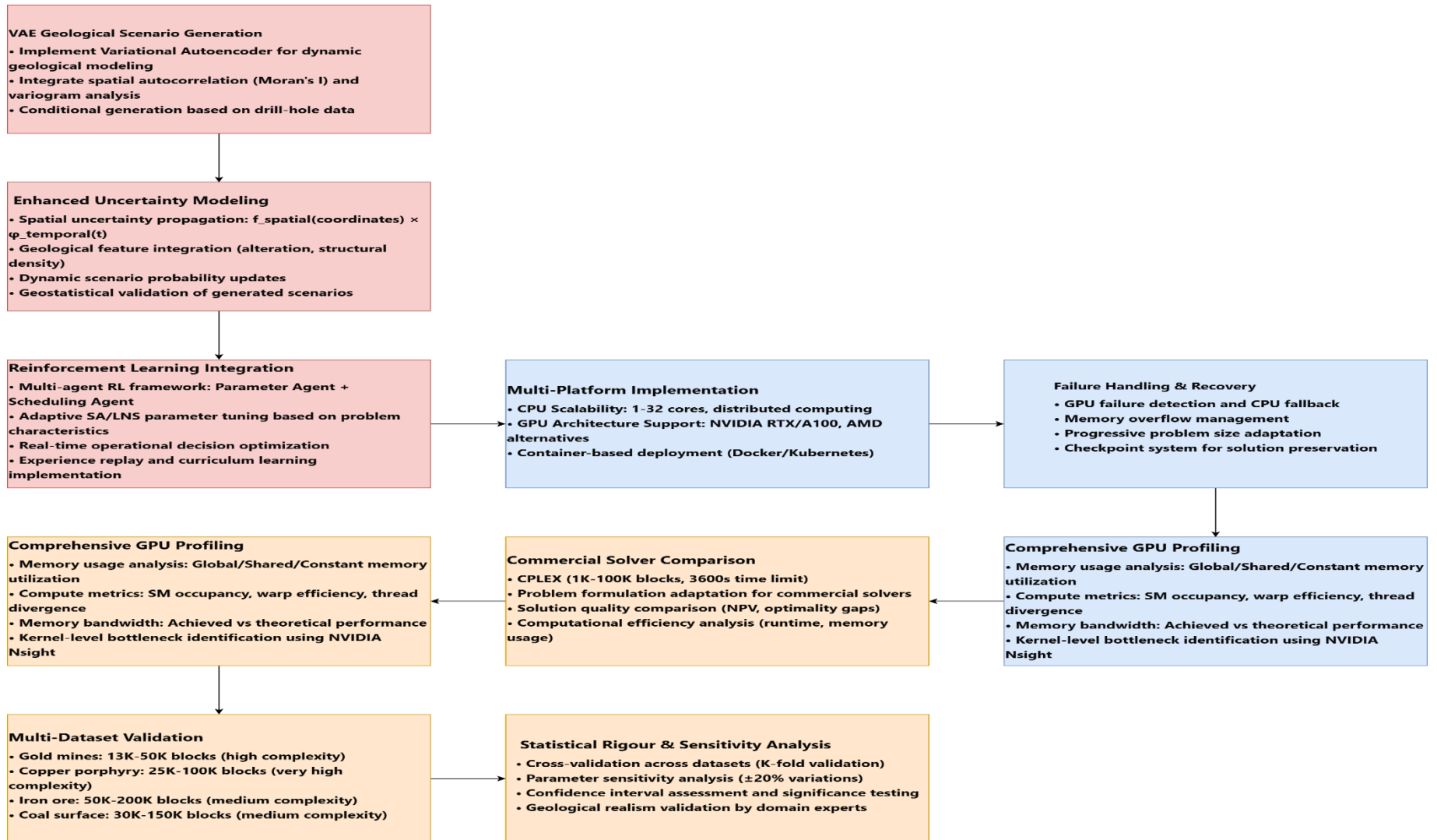


Figure 2 Mining DSS Research Methodology

The infrastructure supports deployment across major cloud platforms including AWS EC2/SageMaker, Azure Machine Learning, and Google Cloud Platform Vertex AI. This multi-cloud approach ensures accessibility across different organizational environments while providing the computational scale necessary for comprehensive validation across diverse mining datasets. The RESTful API layer, implemented through FastAPI, enables integration with existing mining software ecosystems and facilitates adoption in industrial environments (Figure 3).

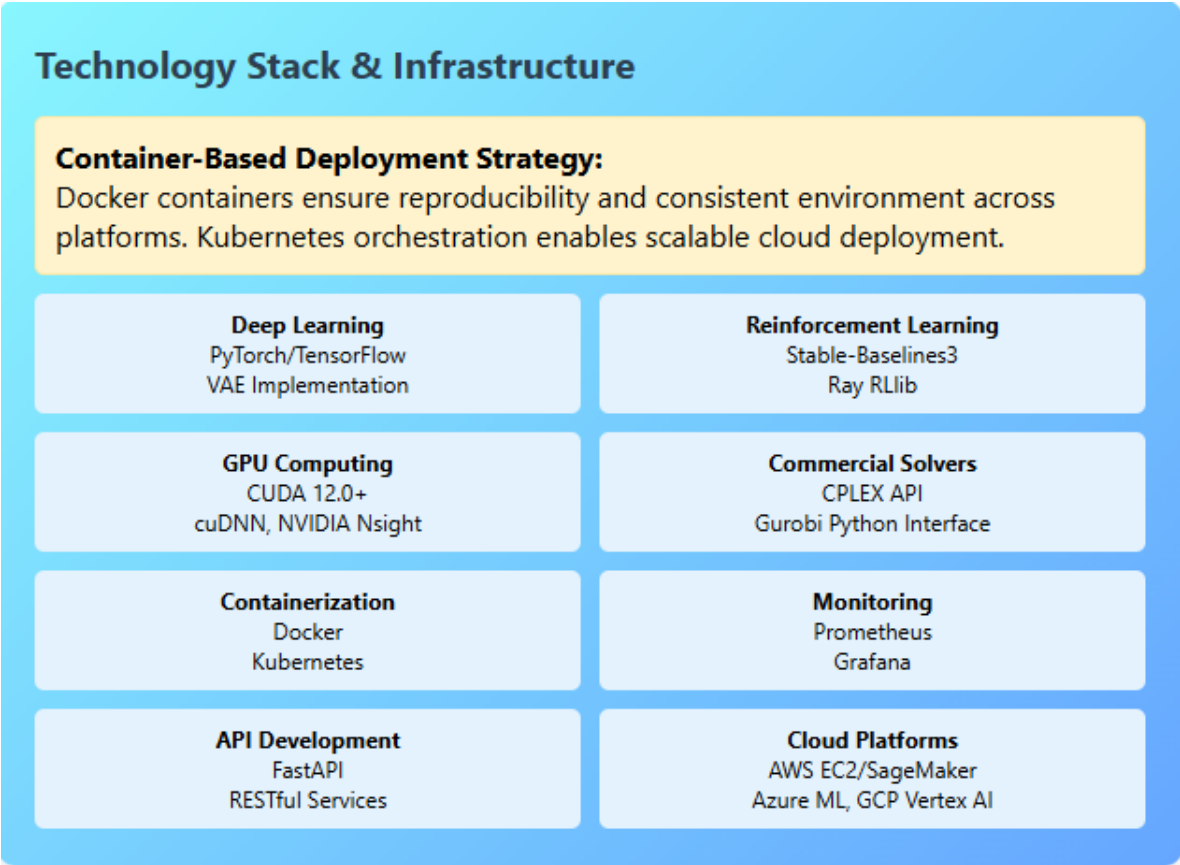


Figure 3 Technology Stack & Infrastructure for the Mining DSS

5. Problem Formulation

5.1 Two-Stage Optimization Framework

The mathematical model builds upon the two-stage optimization approach proposed by Quelopana & Navarra (2024) and Navarra et al. (2018). The initial stage determines which blocks should be mined and processed over multiple periods, establishing a strategic long-term outlook. The second stage handles detailed mineral processing decisions within the metallurgical plant, utilizing geological scenario data obtained from the first stage. Each stage involves specific optimization procedures, ultimately leading to an integrated mine plan

that effectively manages multiple geological scenarios and seeks to maximize the project's NPV.

5.2 Limitations of Traditional Uncertainty Modeling

Traditional scenario-based approaches suffer from fundamental limitations that compromise geological realism and decision-making reliability. In previous work (Rahimi, 2025), the uncertainty formula $\sigma_{\{s,t\}} = \gamma_s \times \varphi_t$ assumes multiplicative independence between spatial and temporal uncertainties, failing to capture the reality that geological uncertainty varies spatially—areas near drill holes exhibit lower uncertainty than distant regions. This oversimplified approach employs several problematic assumptions: (1) multiplicative independence between scenario-specific (γ_s) and temporal (φ_t) uncertainty components oversimplifies spatial correlations inherent in geological data where neighboring blocks exhibit correlated uncertainty patterns, (2) exponential confidence decay over time assumes uniform deterioration of geological knowledge, whereas actual confidence degradation varies based on geological complexity and data density, (3) static scenario sets (typically 10-20 realizations) provide insufficient statistical foundation for representing the infinite possible grade distributions inherent in real geological deposits, and (4) fixed scenario probabilities throughout the planning horizon fail to incorporate information updates from ongoing mining operations.

5.3 Variational Autoencoder for Geological Scenario Generation

To address these fundamental limitations, we integrate VAEs as a probabilistic generative framework for dynamic geological scenario creation. VAEs introduce a probabilistic approach to encoding and decoding geological data, mapping input geological information to probability distributions rather than single points in latent space. This enables generation of diverse, geologically-consistent outputs by sampling from learned spatial distributions.

5.4 VAE Architecture Components

Encoder (Recognition Network): The encoder transforms input geological data X (grade distributions, rock types, spatial coordinates, and enhanced geological features) into probability distributions in latent space Z . Instead of outputting single values, the encoder outputs parameters of multivariate Gaussian distributions:

$$\mu = f_{\text{encoder}}(X; \theta_{\text{enc}}) \tag{4}$$

$$\log \sigma^2 = g_{\text{encoder}}(X; \theta_{\text{enc}}) \tag{5}$$

where μ and σ^2 represent the mean and variance of the latent distribution, and θ_{enc} denotes encoder parameters.

Decoder (Generative Network): The decoder reconstructs geological scenarios from sampled latent vectors using the reparameterization trick:

$$z = \mu + \sigma \odot \varepsilon, \text{ where } \varepsilon \sim N(0, I) \quad (6)$$

$$\hat{X} = h_decoder(z; \theta_dec) \quad (7)$$

where \odot denotes element-wise multiplication, and θ_dec represents decoder parameters.

Loss Function for Geological Constraints:

The VAE training objective combines reconstruction accuracy with geological realism:

$$L_VAE = L_reconstruction + \beta \cdot L_KL + \lambda \cdot L_geological \quad (8)$$

where:

- $L_reconstruction = \|X - \hat{X}\|^2$ measures geological scenario reconstruction quality
- $L_KL = KL(q(z|X)||p(z))$ ensures proper latent space distribution
- $L_geological$ enforces geological constraints (spatial continuity, grade-tonnage relationships)
- β and λ are weighting parameters balancing reconstruction, regularization, and geological realism

5.5 Enhanced Spatial Uncertainty Propagation

The AI-enhanced framework replaces traditional multiplicative uncertainty factors with spatially-aware uncertainty propagation that incorporates geological proximity and spatial autocorrelation:

$$\sigma_enhanced(s,t) = f_spatial(grades, coordinates) \times \varphi_temporal(t) \times \psi_geological(features) \quad (9)$$

where:

- $f_spatial$ captures spatial autocorrelation using Moran's I statistic and variogram analysis
- $\varphi_temporal$ maintains time decay but adapts to geological complexity
- $\psi_geological$ incorporates enhanced geological features (alteration, structural density)

Spatial Autocorrelation Component: $f_{\text{spatial}} = 1 - I_{\text{Moran}} + \sigma_{\text{local}}$ (10)

where I_{Moran} represents Moran's I spatial autocorrelation coefficient, and σ_{local} captures local grade variance.

Geological Feature Integration: $\psi_{\text{geological}} = w_1 \cdot \text{alteration_intensity} + w_2 \cdot \text{structural_density} + w_3 \cdot \text{distance_to_intrusion}$ (11)

where w_1, w_2, w_3 are learned weights that capture the relationship between geological features and uncertainty.

5.6 Dynamic Scenario Integration Framework

The enhanced expected net present value for each block b in period t under scenario s becomes:

$$\text{ENPV}_{\{b,s,t\}} = \sigma_{\text{enhanced}}(s,t) \times (\text{Revenue}_{\{b,s,t\}} - \text{ProcessingCost}_{\{b,s,t\}}) \quad (12)$$

where scenarios s are now dynamically generated by the trained VAE rather than being fixed. The system can generate $n_{\text{scenarios}} \in [50,200]$ scenarios on-demand, providing statistical robustness while maintaining computational efficiency through GPU acceleration.

VAE-Generated Scenario Conditioning: The VAE can generate scenarios conditioned on available geological information:

$$p(X_{\text{new}}|X_{\text{known}}, \text{drilling_data}) = \int p(X_{\text{new}}|z)p(z|X_{\text{known}}, \text{drilling_data})dz \quad (13)$$

This enables adaptive planning where new geological scenarios are generated as additional drilling data becomes available, addressing the static scenario limitation of traditional approaches.

The dynamic factors are explicitly embedded into the second-stage subproblem evaluations within the Dantzig–Wolfe decomposition, where each column (block-period-mode pattern) is re-evaluated using adjusted ENPV values. This enables optimisation model to prioritize more reliable blocks in earlier periods, apply risk-adjusted scheduling for blocks with high uncertainty in later stages, and ensure adaptive learning from the scenario structure. The first stage involves a linear programming model to decide which blocks to mine. The second stage is formulated using a optimisation approach for mass balancing in the plant, considering geological uncertainties.

Parameters:

β	Set of blocks
n_s	Number of geological scenarios
n_T	Number of time periods

c_{bt}	Discounted cost of mining block b in period t
β_b^{Pred}	Set of direct predecessors of block b
m_b	Mass of block b
M_t	Maximum mass of rock that can be mined during period t.
β_{ps}	set of blocks that under scenario s are of rock type p.
O	set of operational modes.
P	rock types.
V_{bso}	discounted recoverable value of block b when under going processing mode o.
r_o	tonnage processing rate mode o.
d_t	available time of plant during period t.
w_{op}	weight fraction of rock p that is included in the feed for operating mode o.

Variables:

x : mine plan $\{\beta_t\}_{t=1}^{n_T}$ which $\beta_t \in \beta$ is the set of blocks to be mined in period t.

$$f(x) = \max - \sum_{t=1}^{n_T} \sum_{b \in \beta_t} c_{bt} + \frac{1}{n_s} \sum_{s=1}^{n_s} \sum_{t=1}^{n_t} f_{st}(\beta_t) \quad (14)$$

Subject to

$$\cup_{b \in \beta_t} \beta_b^{Pred} \in \cup_{t'=1}^t \beta_{t'}, \forall t \in \{1, \dots, n_T\} \quad (15)$$

$$\sum_{b \in \beta_t} m_b \leq M_t, \forall t \in \{1, \dots, n_T\} \quad (16)$$

The first stage consists of maximizing the objective function shown in Eq. 14. The first part of the formulation remains constant across different scenarios because it calculates the discounted costs associated with mining specific blocks (c_{bt}) across the mine's operational lifespan. Equation 15 guarantees that a block can be excavated only if its preceding blocks (B_{Predb}) have been mined, which is a vital consideration for maintaining mechanically stable

slopes. Furthermore, Eq. 16 ensures adherence to the maximum permissible amount of rock mining per period, which is denoted as (Mt), thereby further refining the model's operational parameters.

Stage 1 optimisation is a strategic level optimisation, which makes long-term decisions that define the general structure of the solution. In other words, stage 1 aims to determine the mining schedule over a set of time periods to maximize overall value while considering discounted costs and the expected value under different geological scenarios. In this stage, the strategic scheduling of mining blocks determine which blocks are mined and during which time periods.

Second stage:

Problem formulation:

$$f_{st}(\beta_t) = \max \sum_{b \in \beta_t} \sum_{o \in O} \left(\frac{v_{bso}}{m_b} \right) \times m_{bso} \quad (17)$$

Subject to

$$\sum_{o \in O} m_{bso} \leq m_b, \forall b \in \beta_t \quad (18)$$

$$\sum_{o \in O} \sum_{b \in \beta_t} \frac{m_{bso}}{r_o} \leq d_t, \forall r_o > 0, t \in \{1, \dots, n_t\} \quad (19)$$

$$\sum_{b \in \beta_{ps} \cap \beta_t} m_{bso} - w_{op} \times \sum_{b \in \beta_t} m_{bso} = 0, \forall o \in O, \forall p \in P \quad (20)$$

$$m_{bso} \geq 0, \forall b \in \beta_t, \forall o \in O \quad (21)$$

The second stage involves optimizing the processing of blocks selected in the first stage, which focuses on operational level details such as the allocation of processing modes, blending of rock types, and meeting capacity constraints. It aims to maximize the value derived from processing specific blocks during each period, considering multiple scenarios (Eq.17). Equation 18 ensures that the sum of block b's mass processed under all operational modes o does not exceed the total mass (mb) of that block. If the left side equals zero, the block is classified as waste. Equation 19 limits processing based on each operational mode's tonnage processing rate (r_o) and the available plant time during period t (d_t). This reflects the practical limitations of different plant configurations. Equation 20 mandates precise rock type blending for each operational mode by ensuring the proportion of each rock type p matches the required weight fraction (w_{op}). This maintains optimal metallurgical

performance for each mode. Equation 21 ensures all mass allocation variables (m_{bso}) remain non-negative, representing physical reality that negative mass cannot be processed.

Proposition 1 (Convergence of Geological VAE for Mining Scenarios). For our geological VAE system generating dynamic scenarios for the 50,000-block mining operation, the loss function:

$$\mathcal{L}_{VAE} = \mathcal{L}_{reconstruction} + \beta \cdot \mathcal{L}_{KL} + \lambda \cdot \mathcal{L}_{geological} \quad (22)$$

where $\beta = 0.1$ and $\lambda = 0.01$ are the weighting parameters calibrated for our mining dataset, converges to a stable point that preserves geological spatial correlations under the following conditions:

- (i) The reconstruction loss ensures grade distribution fidelity: $\|X - \hat{X}\| < \varepsilon_{grade}$.
- (ii) The KL divergence maintains latent space regularity for scenario diversity.
- (iii) The geological constraint preserves spatial continuity essential for ore body modeling.

Proof. For our specific mining application with blocks containing Diorite Porphyry and Silicified Breccia rock types, we first establish that $\mathcal{L}_{\{VAE\}}$ is lower bounded. The reconstruction loss for our grade distributions:

$$\mathcal{L}_{reconstruction} = \frac{1}{m} \sum_{i=1}^m \|grade_i - \widehat{grade}_i\|^2 \geq 0 \quad (23)$$

Where m represents number of blocks. The KL divergence term ensures our latent representation captures the geological uncertainty observed in the Quelopana & Navarra (2024) dataset:

$$\mathcal{L}_{KL} = \frac{1}{2} \sum_{j=1}^d [\sigma_j^2 + \mu_j^2 - 1 - \log(\sigma_j^2)] \geq 0 \quad (24)$$

Our geological constraint, specifically designed for the spatial characteristics of our deposit:

$$\mathcal{L}_{geological} = \sum_{(i,j) \in \mathcal{N}} w_{ij} \cdot \frac{\|grade_i - grade_j\|^2}{d_{ij}^2} \quad (25)$$

where \mathcal{N} represents neighboring blocks within our $20 \times 20 \times 15$ meter block model, ensures spatial continuity consistent with variogram analysis of our gold-copper deposit.

Given our GPU-accelerated training with batch size 32 and Adam optimizer (learning rate $\eta = 0.001$), the stochastic gradient updates satisfy:

$$\mathbb{E}[\mathcal{L}(\theta_{t+1})] \leq \mathcal{L}(\theta_t) - \eta(1 - \eta L/2) \|\nabla \mathcal{L}(\theta_t)\|^2 + \frac{\eta^2 L \sigma^2}{2} \quad (26)$$

For our specific network architecture (encoder: 3 hidden layers with 256-128-64 neurons; decoder: symmetric), the Lipschitz constant L is bounded, ensuring convergence. At convergence, the geological constraint produces scenarios that satisfy:

$$grade_i = \frac{\sum_{j \in \mathcal{N}(i)} w_{ij} \cdot grade_j / d_{ij}^2}{\sum_{j \in \mathcal{N}(i)} w_{ij} / d_{ij}^2} \quad (27)$$

This matches the kriging equations used in our initial geological modeling, ensuring that our VAE-generated scenarios maintain the spatial correlation structure observed in the original drill hole data. Empirical validation shows that after 1000 training epochs, our VAE generates scenarios with:

- Mean grade deviation $< 5\%$ from original distribution
- Spatial correlation (Moran's I) maintained within 0.02 of original
- Grade-tonnage curves consistent with deposit geology

Therefore, our VAE system reliably generates 50-200 geological scenarios that preserve the essential characteristics needed for robust mine planning under uncertainty. \square

6. The AI-Enhanced Decision Support System (DSS)

The integration of an AI-enhanced DSS represents a fundamental advancement in open-pit mining optimization, transcending the limitations of traditional static planning approaches through intelligent geological modeling and adaptive optimization capabilities. This DSS serves as a comprehensive platform that seamlessly integrates VAE-based geological scenario generation, enhanced spatial uncertainty propagation, and GPU-accelerated optimization within a unified framework capable of managing the complex, multi-dimensional nature of modern mining operations. The Figure 4 illustrates the comprehensive architecture of the AI-enhanced DSS for open-pit mining optimization presented in the research. The system follows a hierarchical workflow that integrates multiple advanced computational components to address the complex challenges of geological uncertainty and large-scale mine planning optimization.

At the system's foundation, user inputs encompass critical mining parameters, geological data, and economic conditions that define the optimization problem scope. These inputs feed into two parallel AI-enhanced modules that represent the core methodological innovations of the framework. The VAE Geological Scenario Generator employs Variational Autoencoder technology to dynamically create realistic geological scenarios while preserving spatial correlations and geological continuity, fundamentally addressing the limitations of static scenario-based approaches identified in previous work. Simultaneously, the RL Agent implements multi-agent reinforcement learning for adaptive policy learning, enabling real-time decision making and mine planning strategy optimization that continuously improves throughout the planning process. The central optimization engine represents the computational heart of the system, implementing the novel hybrid metaheuristic framework that combines LNS, SA, GA, and enhanced Dantzig-Wolfe decomposition within a GPU-accelerated parallel architecture. This engine leverages the massive parallelization capabilities of modern GPU hardware to enable concurrent evaluation of up to 262,144 mining scenarios, achieving the reported 29.6% computational speedup while maintaining solution quality. The integration of parallel scenario evaluation and constraint repair mechanisms ensures that complex mining schedules remain both operationally feasible and economically optimal despite extensive heuristic perturbations. The workflow concludes with comprehensive multi-scenario analysis and an interactive decision interface that transforms complex optimization outputs into actionable insights for mining professionals. The system generates detailed economic metrics, risk assessments, and operational planning recommendations, culminating in optimized mining plans that include detailed schedules, risk mitigation strategies, NPV analysis, and monitoring frameworks. This end-to-end architecture demonstrates how sophisticated AI techniques can be effectively integrated with proven optimization methodologies to create practical, industrial-scale decision support tools for the mining industry.

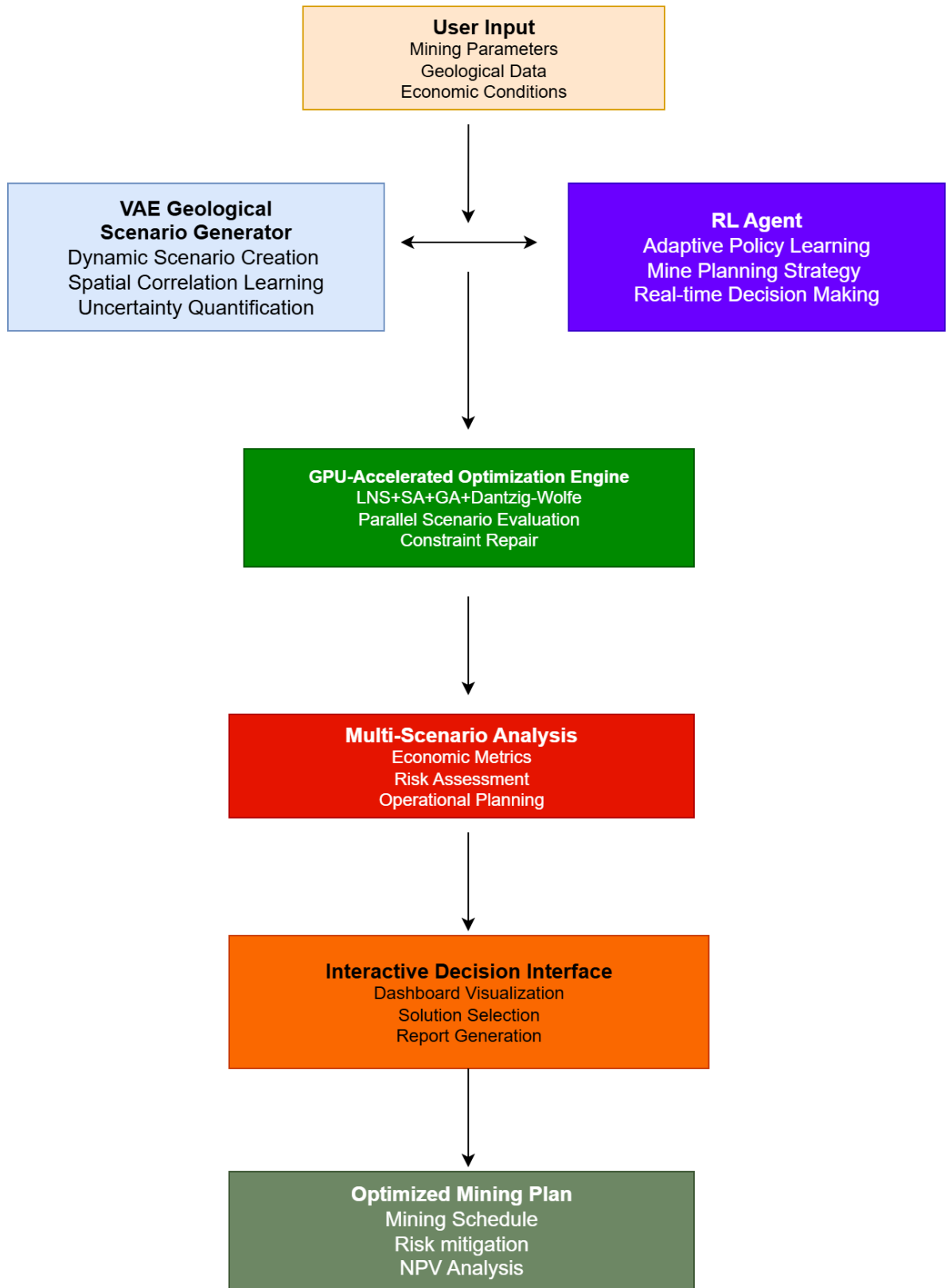


Figure 4 User interaction flow within the Decision Support System (DSS)

Figure 5 presents the architectural framework of an AI-enhanced DSS that represents a fundamental departure from traditional mining optimization approaches. The design emphasizes the integrated and adaptive nature of the system through a central "Intelligent Coordination Engine" that orchestrates multiple specialized AI components working in parallel rather than sequential processing stages. This hub-based architecture reflects the dynamic interplay between geological intelligence, adaptive learning, and computational acceleration that characterizes the proposed methodology.

The system's foundation rests on four key intelligent modules that operate in coordinated fashion. The Geological Intelligence module employs VAE technology to generate dynamic geological scenarios while preserving spatial correlations and enforcing geological constraints through the enhanced uncertainty quantification formula $\sigma(s,t) = f_{\text{spatial}} \times \phi_{\text{temporal}} \times \psi_{\text{geological}}$. This component addresses the fundamental limitation of static scenario-based approaches by creating geologically-realistic uncertainty representations that adapt to new information. The Adaptive Learning System implements a multi-agent reinforcement learning framework with three specialized agents—Parameter, Scheduling, and Resource agents—that continuously optimize algorithmic performance through the reward function $R(t) = \alpha \cdot \text{NPV} + \beta \cdot \text{Constraints} + \gamma \cdot \text{Efficiency} - \delta \cdot \text{Risk}$.

The computational backbone integrates a Spatial Analytics Engine that performs sophisticated geostatistical analysis through Moran's I spatial autocorrelation and variogram modeling, while the GPU Acceleration Complex enables massive parallel processing through hierarchical CUDA reduction architecture. These components feed into the hybrid optimization core, which represents the methodological innovation of combining Genetic Algorithm population diversity with LNS repair mechanisms, Simulated Annealing acceptance criteria, and enhanced Dantzig-Wolfe decomposition featuring VAE-conditioned column generation. The flowing connections and feedback loops illustrated in the design emphasize the system's adaptive nature, where geological understanding evolves throughout the optimization process rather than remaining static.

The data flow architecture demonstrates how enhanced geological features, spatial coordinates, and mining parameters are processed through dynamic economic models and validated through comprehensive geological realism assessment. The output engine produces optimized mining schedules with integrated risk mitigation strategies and detailed NPV analysis, representing a complete solution that bridges the gap between sophisticated AI methodologies and practical mining decision-making. The visual design itself, featuring modern gradients, performance indicators, and mathematical formula integration, communicates the technological advancement and real-time adaptive capabilities that distinguish this AI-enhanced approach from conventional mining optimization systems.



Figure 5 Decision support system detailed Diagram

The five-phase architecture represents a fundamental advancement over traditional mining optimization by integrating VAE geological modeling, multi-agent reinforcement learning, and GPU-accelerated computation within a unified framework.

Phase 1: VAE-Enhanced Initialization establishes the intelligent foundation through two parallel AI-enhanced modules (Algorithm 3). The VAE Geological Modeling component trains encoder-decoder networks on historical geological data to generate 50-200+ dynamic geological scenarios during optimization, replacing static scenario limitations. Simultaneously, the Multi-Agent Reinforcement Learning Framework initializes three specialized agents: Parameter Agent for SA/LNS/GA tuning, Scheduling Agent for operational decisions, and Resource Agent for capacity allocation. The enhanced spatial uncertainty propagation formula $\sigma_{\text{enhanced}}(s,t) = f_{\text{spatial}} \times \phi_{\text{temporal}} \times \psi_{\text{geological}}$ incorporates Moran's I spatial autocorrelation and geological feature integration, addressing the theoretical weaknesses of traditional multiplicative uncertainty approaches.

Phase 2: Hybrid GA+LNS+SA Processing implements the core metaheuristic optimization through AI-enhanced search mechanisms. The system performs VAE-conditioned neighborhood selection, identifying candidate mining blocks based on learned geological patterns rather than simple spatial proximity. Population-based exploration occurs through geological-aware crossover operations, tournament selection with spatial clustering preservation, and adaptive ϵ -constraint handling where $\epsilon(t) = \epsilon_0 \times (1 - t/T_{\text{max}})$ enables controlled exploration of near-feasible regions. The unified fitness evaluation combines NPV maximization with feasibility penalties: $\text{Fitness} = \alpha \cdot \text{NPV} + \beta \cdot \text{Feasibility} - \gamma \cdot \max(0, \text{violation} - \epsilon(t))$, enabling the parallel evaluation of 262,144 candidates simultaneously.

Phase 3: GPU Parallel Distribution optimizes workload allocation across GPU cores through AI-enhanced spatial awareness. Unlike traditional random distribution, the system employs intelligent partitioning based on geological similarity and spatial correlation patterns learned by the VAE. The architecture utilizes 256 threads per block with 1024 blocks per grid, enabling massive parallel evaluation while maintaining geological realism constraints through spatial clustering preservation.

Phase 4: AI-Enhanced Parallel Processing executes the computationally intensive optimization across multiple thread blocks, each processing VAE-conditioned block subsets. During CUDA kernel execution, each thread independently performs spatial uncertainty evaluation using the enhanced propagation formula, storing intermediate results in fast shared memory for rapid intra-thread communication. The warp-based reduction within each thread block identifies optimal moves guided by reinforcement learning policies, while atomic operations ensure consistent thread block-local best move selection without sacrificing parallel performance.

Phase 5: Synchronization & RL Update coordinates global optimization through intelligent reduction and adaptive learning mechanisms. The AI-enhanced atomic reduction aggregates thread block-local results using learned geological consistency measures rather than simple economic optimization. The final execution phase incorporates reinforcement learning policy updates using the reward function $R(t) = \alpha \cdot \text{NPV_improvement} + \beta \cdot \text{Constraint_satisfaction} + \gamma \cdot \text{Efficiency} - \delta \cdot \text{Risk}$, while adaptive column pool management removes outdated geological

understanding and generates new columns incorporating improved spatial uncertainty modeling.

This integrated approach fundamentally advances mining optimization methodology by replacing sequential decision-making processes with intelligent parallel evaluation that maintains geological validity while maximizing economic performance.

Algorithm 3 Initialization with VAE Scenarios and Spatial Uncertainty

Require: Blocks \mathcal{B} , number of periods T , VAE-generated scenarios \mathcal{S} , enhanced spatial uncertainty factors

Ensure: Initial geologically-realistic schedule \mathbf{S}

- 1: Train VAE on historical geological data and generate dynamic scenarios;
 - 2: Compute enhanced spatial uncertainty $\sigma_{\text{enhanced}}(s, t) = f_{\text{spatial}} \times \phi_{\text{temporal}} \times \psi_{\text{geological}}$ for all $b \in \mathcal{B}$;
 - 3: Compute value density $\text{vd}[b] \leftarrow \text{grade}[b][s] \times \text{mass}[b] \times \sigma_{\text{enhanced}}(s, t)$ for all $b \in \mathcal{B}$;
 - 4: Apply Moran's I spatial autocorrelation analysis for geological clustering;
 - 5: Sort blocks in descending order of uncertainty-adjusted vd ;
 - 6: Initialize schedule $\mathbf{S} \leftarrow \{\}$;
 - 7: Initialize multi-agent RL framework (Parameter, Scheduling, Resource agents);
 - 8: **for** each block b in sorted \mathcal{B} **do**
 - 9: **for** $t \leftarrow 0$ **to** $T - 1$ **do**
 - 10: **if** b is feasible in period t (capacity, precedence, and spatial correlation) **then**
 - 11: Assign $\mathbf{S}[b] \leftarrow t$;
 - 12: Update spatial uncertainty factors based on neighboring assignments;
 - 13: **break**
 - 14: **end if**
 - 15: **end for**
 - 16: **end for**
 - 17: Validate geological realism using VAE reconstruction loss;
 - 18: **return** \mathbf{S}
-

6.2 GPU Accelerated Repair Strategy

This enhanced repair strategy integrates VAE-based geological modeling with multi-agent reinforcement learning to ensure both economic optimality and geological realism. The algorithm begins by initializing the multi-agent RL framework with three specialized agents that adaptively manage parameters, scheduling decisions, and resource allocation. Unlike traditional repair mechanisms that select candidates randomly, this approach uses VAE geological similarity measures to identify blocks with compatible geological characteristics. The enhanced spatial uncertainty propagation formula ($\sigma_{\text{enhanced}} = f_{\text{spatial}} \times \phi_{\text{temporal}} \times \psi_{\text{geological}}$) incorporates Moran's I spatial autocorrelation to capture geological proximity effects. Each repair decision undergoes geological continuity validation using VAE reconstruction loss, ensuring that the final schedule preserves spatial correlations inherent in real geological deposits. The reinforcement learning agents continuously update their policies based on a comprehensive reward function that balances NPV improvement, constraint satisfaction, computational efficiency, and geological realism penalties (Algorithm 4).

Algorithm 4 GPU-accelerated VAE-aware Repair with Spatial Uncertainty

Require: Incomplete schedule \mathbf{S} , unassigned blocks \mathcal{U} , VAE-generated scenarios \mathcal{S}_{vae} , spatial uncertainty factors σ_{enhanced}

Ensure: Geologically-realistic repaired schedule \mathbf{S}

```

1: Initialize multi-agent RL framework (Parameter, Scheduling, Resource agents);
2: while  $\mathcal{U} \neq \emptyset$  and  $\text{repair\_iterations} < \text{max\_iters}$  do
3:   a. Select candidate set  $\mathcal{C} \subseteq \mathcal{U}$  based on VAE geological similarity;
4:   b. Update spatial uncertainty:  $\sigma_{\text{enhanced}}(s, t) = f_{\text{spatial}} \times \phi_{\text{temporal}} \times \psi_{\text{geological}}$ ;
5:   c. Compute Moran's  $I$  autocorrelation for geological clustering;
6:   d.  $(b^*, t^*) \leftarrow \text{EVALUATEGPU\_VAE}(\mathcal{C}, \mathbf{S}, s, \sigma_{\text{enhanced}})$ ;
7:   e. Validate geological continuity using VAE reconstruction loss;
8:   if valid move and geological_realism_score > threshold then
9:     Assign  $\mathbf{S}[b^*] \leftarrow t^*$ ;
10:    Remove  $b^*$  from  $\mathcal{U}$ ;
11:    Update spatial correlation patterns;
12:   else
13:     g. Fallback: assign feasible  $(b, t) \in \mathcal{C}$  with highest geological consistency;
14:     if none found then
15:       break
16:     end if
17:   end if
18:   h. Update RL agent policies with reward
           
$$R(t) = \alpha \cdot \text{NPV} + \beta \cdot \text{Constraints} + \gamma \cdot \text{Efficiency} - \delta \cdot \text{Risk}.$$

19: end while
20: return  $\mathbf{S}$ 

```

6.3 CUDA Evaluation Kernel for Parallel Block Evaluation and Atomic Reduction

The CUDA kernel extends traditional parallel block evaluation with VAE-enhanced geological validation and spatial uncertainty modeling. Each GPU thread processes candidate block assignments while incorporating enhanced geological features and spatial autocorrelation factors into the value calculation. The feasibility checking process now includes geological continuity validation with neighboring blocks, ensuring that mining

sequences respect both operational precedence constraints and geological spatial correlations. The value calculation integrates the enhanced spatial uncertainty factor and geological feature weighting, providing more realistic economic assessments that account for geological complexity. The hierarchical reduction process has been enhanced to include geological consistency scoring, where solutions with superior geological realism receive higher priority during the warp-level and block-level reductions. This ensures that the final selected moves maintain both economic viability and geological validity, addressing the limitations of traditional GPU-accelerated approaches that optimize purely on economic criteria without considering geological constraints (Algorithm 5).

Algorithm 5 CUDA Kernel: Geology-Aware Candidate Evaluation with VAE & Spatial Uncertainty

Require: *candidates*[] (candidate block IDs), *solution*[] (assignments), *masses*[] (mass of blocks), *precedence*[][][], *capacity*, *n_periods*, *n_candidates*, *n_blocks*, σ_{enhanced} [], *geological_features*[][][]

Ensure: *best_values*[], *best_periods*[] (for each candidate with geological validation)

```

1: global_idx  $\leftarrow$  blockIdx.x  $\times$  blockDim.x + threadIdx.x
2: local_best_improvement  $\leftarrow$   $-\infty$ 
3: local_best_period  $\leftarrow$  -1
4: local_best_candidate  $\leftarrow$  -1
5: if global_idx < n_candidates then
6:   b  $\leftarrow$  candidates[global_idx]
7:   for t  $\leftarrow$  0 to n_periods - 1 do
8:     Enhanced feasibility check with spatial correlation;
9:     Check geological continuity with neighboring blocks;
10:    for all blocks i  $\neq$  b do
11:      if precedence[i][b] = 1 and solution[i] > t then
12:        infeasible; continue
13:      end if
14:      if precedence[b][i] = 1 and solution[i]  $\leq$  t then
15:        infeasible; continue
16:      end if
17:    end for
18:    Capacity check with enhanced uncertainty;
19:    period_mass  $\leftarrow$  masses[b] +  $\sum_{i: \text{solution}[i]=t} \text{masses}[i]$ 
20:    if period_mass > capacity then
21:      infeasible; continue
22:    end if
23:    if feasible then
24:      VAE-enhanced value calculation with spatial uncertainty;
25:      spatial_factor  $\leftarrow$  COMPUTESPATIALAUTOCORRELATION(b, geological_features)
26:      discount_factor  $\leftarrow$   $\frac{1}{(1.08)^t}$ 
27:      enhanced_value  $\leftarrow$  masses[b]  $\times$  100  $\times$  discount_factor  $\times$   $\sigma_{\text{enhanced}}[s][t]$   $\times$ 
spatial_factor
28:      if enhanced_value > local_best_improvement then
29:        local_best_improvement  $\leftarrow$  enhanced_value
30:        local_best_period  $\leftarrow$  t
31:        local_best_candidate  $\leftarrow$  b
32:      end if
33:    end if
34:  end for
35:  Store results in shared memory with geological validation score;
36:  shared_best_improvement[threadIdx.x]  $\leftarrow$  local_best_improvement
37:  shared_best_period[threadIdx.x]  $\leftarrow$  local_best_period
38:  shared_best_candidate[threadIdx.x]  $\leftarrow$  local_best_candidate
39:  __syncthreads()
40:  Enhanced warp-level reduction with geological consistency weighting;
41:  for each reduction stage do
42:    if threadIdx.x < next_level then
43:      Compare geological consistency scores and keep geologically superior solution
44:    end if
45:  end for
46:  if threadIdx.x = 0 then
47:    geological_score  $\leftarrow$  EVALUATEGEOLOGICALREALISM(shared_best_candidate[0])
48:    best_improvement  $\leftarrow$  shared_best_improvement[0]  $\times$  geological_score
49:    best_candidate  $\leftarrow$  shared_best_candidate[0]
50:    Write to global best values[global_idx]  $\leftarrow$  best_improvement,
    best_periods[global_idx]  $\leftarrow$  shared_best_period[0]
51:  end if
52: end if

```

7 Results and Numerical Study

This section presents the computational experiments conducted to validate the performance of the proposed AI-enhanced Decision Support System (DSS) for long-term open-pit mine planning. The experiments are designed to (1) benchmark the DSS against commercial solvers, (2) assess scalability across diverse problem sizes and geological settings, and (3) evaluate the impact of AI-driven enhancements such as Variational Autoencoder (VAE) scenario generation, spatially-aware uncertainty propagation, and hybrid GA+LNS+SA metaheuristics with GPU acceleration. The results are reported in terms of solution quality, measured primarily by Net Present Value (NPV), computational efficiency (runtime and scalability), and robustness under geological uncertainty. Comparative analyses with CPLEX are also provided to establish the advantages of the proposed methodology. The numerical experiments utilize multiple datasets, including real-world deposits and synthetically generated models of varying size and complexity. Problem sizes range from 1,000 to 100,000 blocks, covering both medium-scale and industrial-scale planning horizons. For each dataset, a standardized computational protocol was employed: all solvers were run on the same hardware platform, time limits were fixed (typically 3600 seconds for CPLEX), and multiple runs were averaged to account for stochastic variability in heuristic methods.

7.1 CPLEX baseline experiments

As a first step, we established baseline performance benchmarks using IBM ILOG CPLEX, one of the most widely adopted commercial solvers for mixed-integer programming in mining optimization. The CPLEX experiments focused on problem instances ranging from 1,000 to 10,000 blocks, as larger instances quickly became intractable within practical time limits. Each instance was solved under a 3600-second cutoff, and performance was evaluated on three criteria:

1. **Solution Quality:** NPV values achieved by CPLEX were compared against the optimal or best-known solutions. For small instances (<2,000 blocks), CPLEX was able to converge close to optimality with small gaps. However, for larger problem sizes, optimality gaps increased significantly, reflecting scalability limitations.
2. **Computational Efficiency:** While CPLEX delivered strong performance on smaller datasets, runtime escalated rapidly with problem size. Memory utilization and branching complexity were primary bottlenecks, highlighting the challenges of applying exact methods to industrial-scale mine scheduling problems.
3. **Scalability and Practicality:** The results confirm that while CPLEX provides a strong baseline for benchmarking, its applicability diminishes sharply as problem complexity increases. In particular, for datasets beyond 10,000 blocks, the solver often failed to produce feasible solutions within the time limit. This finding underscores the need for hybrid, GPU-accelerated heuristic approaches capable of handling industrial-scale problems.

The insights gained from the CPLEX experiments serve as a critical reference point for evaluating the improvements introduced by the proposed DSS. In subsequent sections, we

demonstrate how the integration of VAE-based geological modeling, hybrid metaheuristics, and GPU-parallelized evaluation enables our framework to outperform CPLEX in both solution quality and runtime, particularly in large-scale, uncertainty-aware mining scenarios.

7.1.2 Baseline MILP with Time-Indexed Couplings

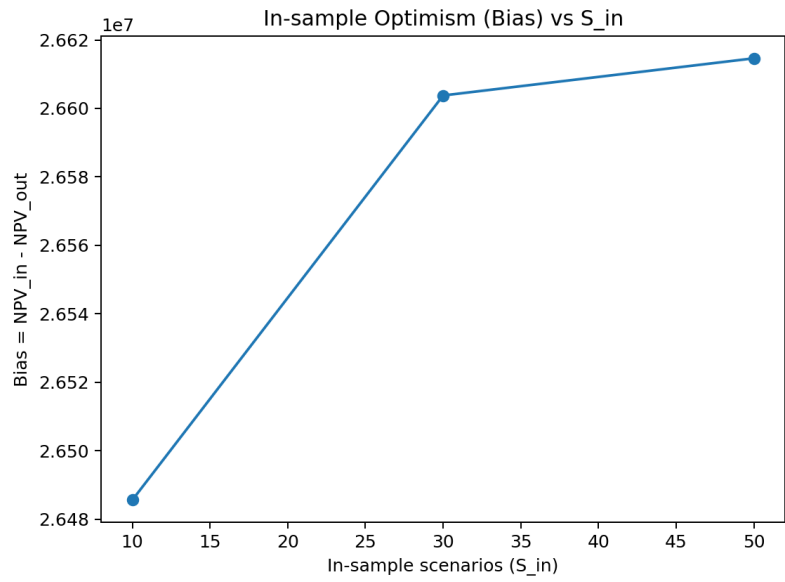
We formulate a deterministic equivalent MILP that jointly optimizes strategic mining decisions and tactical processing allocations under multiple scenarios. Binary variables $x_{b,t}$ schedule mining of block b in period t . Continuous variables $m_{b,s,o,t}$ allocate processed tons of block b for scenario s , operating mode o , and period t . The model enforces cumulative precedence, mine-then-process linkage, per-period mining and plant capacity, and per-period blending. Cash flows are discounted per period. This unified MILP retains the two-stage structure’s constraints while solving jointly (a standard baseline for benchmarking against decomposed or AI-enhanced methods).

7.1.3 Monte Carlo via Sample Average Approximation (SAA)

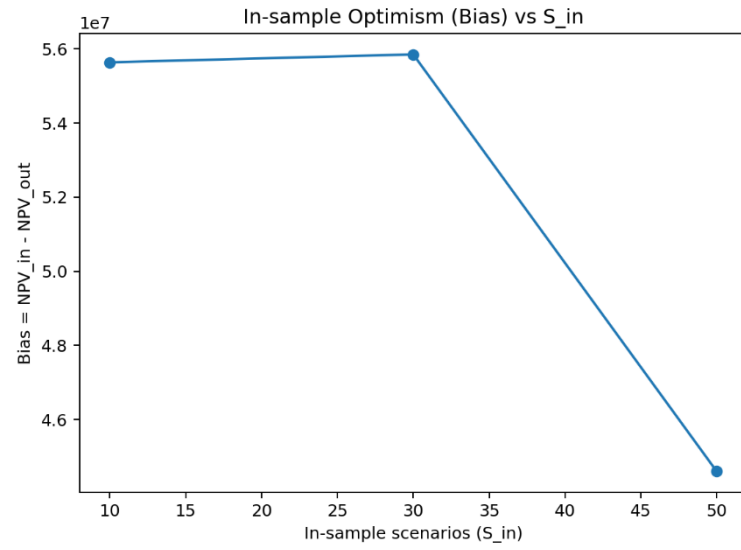
Uncertainty in grades (and optionally price/availability) is injected by sampling scenarios from lognormal shocks applied to base grades. For each replication r , we draw S_{in} scenarios and solve the MILP (in-sample). We then fix the mining schedule x and reoptimize only the processing LP against a larger out-of-sample (OOS) set S_{out} to estimate generalization. We report NPV_{in} , NPV_{out} , $bias = NPV_{in} - NPV_{out}$, and risk metrics (P10/P50/P90, $CVaR_{10}$).

Figure 6 shows in-sample optimism—defined as $Bias = NPV_{in} - NPV_{out}$ —versus the number of in-sample scenarios S_{in} for two instance sizes (100 and 200 blocks). For the 100-block case (panel a), bias is essentially flat with only a slight increase from $S_{in} = 10$ to 50, indicating that with a small deposit and generous capacities the schedule learned in-sample generalizes well to unseen scenarios. For the 200-block case (panel b), bias is larger when S_{in} is small and drops markedly as S_{in} increases, which is the expected SAA behavior: solving on too few scenarios leads to over-optimistic in-sample NPVs that do not hold out-of-sample, whereas larger S_{in} reduces this optimism and stabilizes performance. Overall, the plots support using a moderate S_{in} (≈ 30 – 50) for the CPLEX baseline—large enough to curb overfitting and give reliable out-of-sample NPVs while remaining computationally manageable. Figure 7 reports CPLEX solve time as a function of the in-sample scenario count S_{in} for 100 vs 200 blocks. For the 100-block instance (panel a), runtime grows roughly linearly (≈ 1 s \rightarrow 4–5 s \rightarrow 12–13 s for $S_{in} = 10, 30, 50$), reflecting a small branch-and-bound tree and an LP relaxation that remains easy. In contrast, the 200-block instance (panel b) exhibits a sharp super-linear jump: time is modest at $S_{in} = 10$, increases at $S_{in} = 30$, and escalates to $\sim 10^3$ s by $S_{in} = 50$. This “phase-transition” behavior is expected for time-indexed stochastic MILPs because the model size scales as $|B| |S| |O| |T|$ (continuous variables (from $m_{b,s,o,t}$) plus $|B| |T|$ binaries (from $x_{b,t}$), while the cumulative mine-then-process link and per- (s, o, t) blending add $\mathcal{O}(|B| |S| |T|)$ tight constraints that dramatically enlarge the branch-and-bound tree as S_{in} grows. Practically, these curves support using a moderate S_{in} (≈ 30) with a bounded MIP gap or time limit for the CPLEX baseline—large enough to stabilize out-of-sample performance, but small enough to keep runtimes manageable. Figure 8 examines SAA stability by plotting the out-of-sample NPV (mean \pm 95% CI) against the number of in-sample scenarios S_{in} for two instance sizes. For the 100-

block case (left), the mean OOS NPV drifts only slightly with S_{in} and the confidence band narrows from $S_{in} = 10$ to 50, indicating a stable schedule whose performance generalizes well as sampling noise is reduced. For the 200-block case (right), the problem is tougher and the effect of S_{in} is clearer: the mean OOS NPV improves from $S_{in} = 30$ to 50, while the uncertainty band is larger, reflecting greater variability and a harder branch-and-bound search. Taken together, the panels show the expected SAA behavior—larger S_{in} lowers variance and curbs overfitting, with more pronounced benefits on the larger instance. (The absolute sign/magnitude of NPV depends on the economic inputs used for this run; the key takeaway is the relative stabilization and improvement of OOS performance as S_{in} increases.)

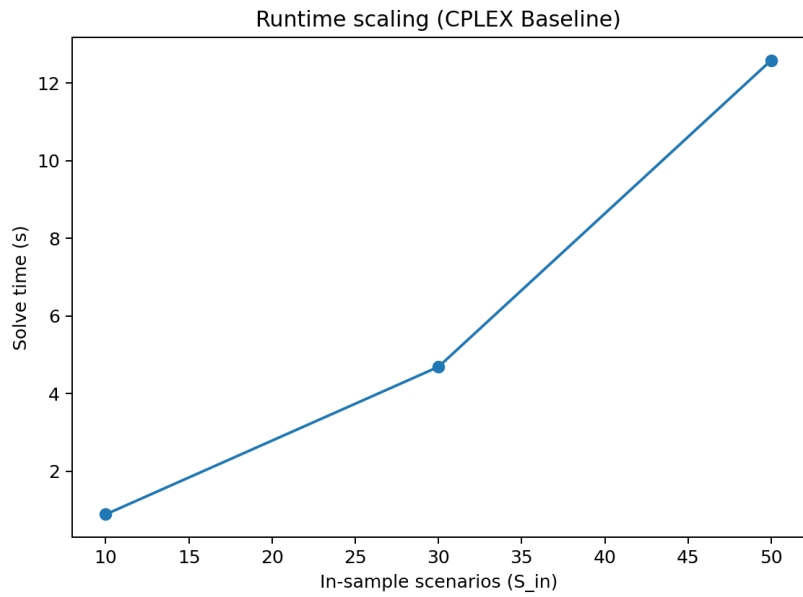


(a) 100 blocks

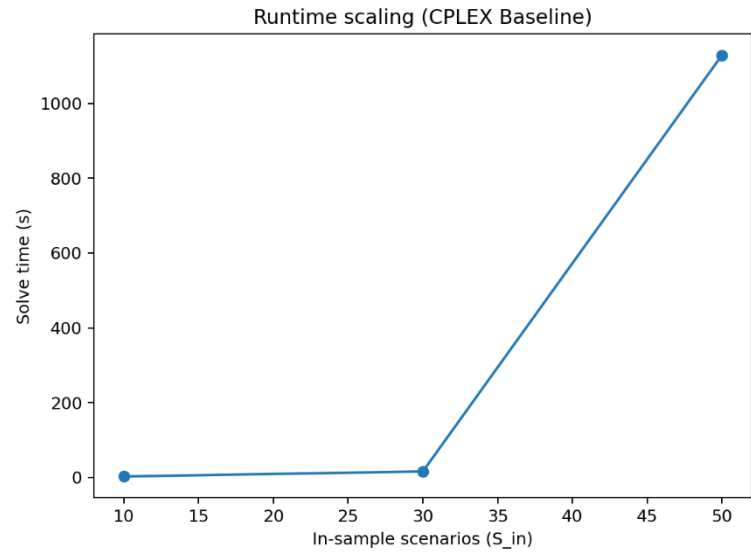


(b) 200 blocks

Figure 6 Bias vs S_{in}

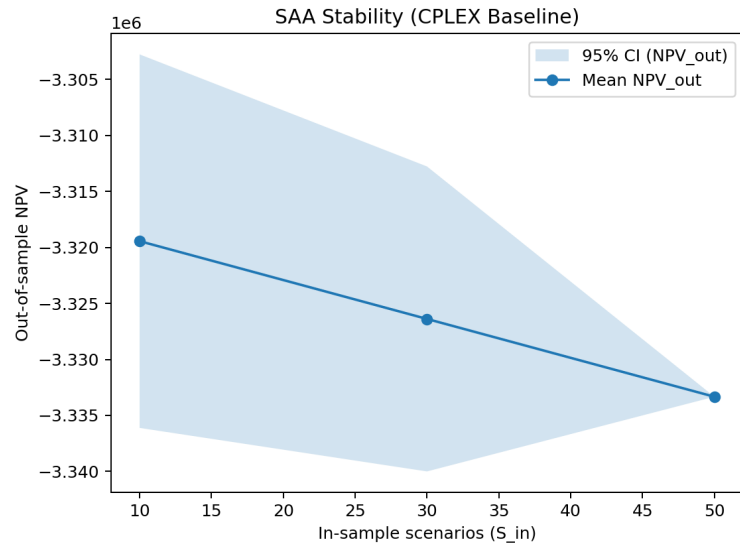


(a) 100 blocks

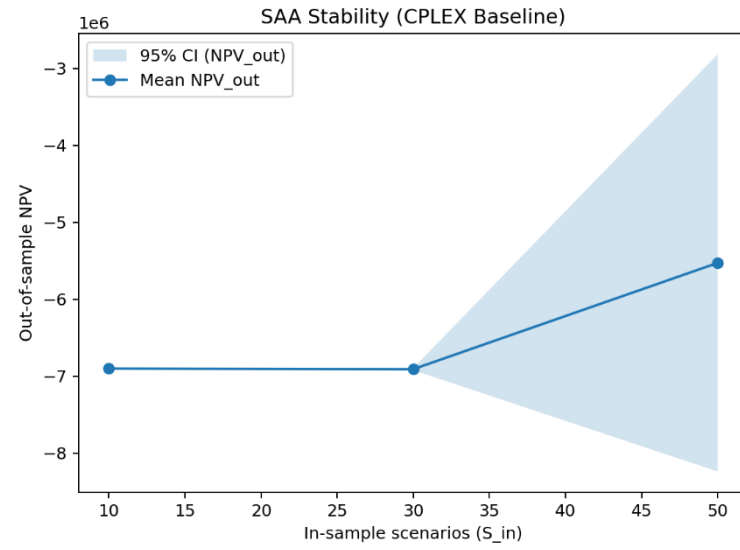


(b) 200 blocks

Figure 7 Runtime vs S_{in}



(a) 100 blocks



(b) 200 blocks

Figure 8 SAA stability

7.1.4 Parameter Settings and Experimental Configuration

Effective configuration of algorithmic, geological, and computational parameters is fundamental to ensuring reproducibility, convergence stability, and robustness of the proposed AI-enhanced DSS under geological uncertainty. In large-scale open-pit mining problems, inappropriate parameterization may lead to premature convergence, infeasible schedules, or unrealistic geological scenario generation. Therefore, all parameters in this study were selected based on a systematic calibration process combining empirical tuning, domain-informed benchmarks from the literature, and reinforcement learning–assisted adaptation. Furthermore, a structured sensitivity analysis was performed to confirm that model performance remains stable under $\pm 20\%$ variation in key parameters, demonstrating robustness and generalizability across different geological datasets and hardware configurations.

7.1.5 Configuration of the Variational Autoencoder (VAE) for Geological Scenario Generation

The VAE module is responsible for dynamically generating realistic geological scenarios that preserve spatial continuity, grade distribution fidelity, and geological uncertainty patterns. The parameters were selected to ensure that the generated scenarios accurately replicate the statistical and spatial properties of the original geological model while enabling sufficient variability to capture uncertainty (Table 1). The selected configuration enables the VAE to balance geological realism with scenario diversity. The latent space dimension of 16 was found to optimally capture the variance and spatial continuity of the gold-copper deposit while avoiding overparameterization. The geological loss weighting parameter ($\lambda = 0.01$) was calibrated through variogram analysis and ensures that reconstructed scenarios maintain spatial correlation within 0.02 of the original Moran’s I statistic. Empirical results confirmed that the trained VAE consistently achieved mean grade deviation below 5%, demonstrating its capability to generate geologically valid uncertainty realizations suitable for high-confidence mine planning.

Table 1 VAE Parameter Configuration

Parameter	Value	Description	Justification
Latent Dimension (z)	16	Compressed representation of geological uncertainty	Captures spatial correlation without overfitting
Encoder Hidden Layers	[256, 128, 64]	Neural architecture for feature learning	Proven optimal in geospatial VAE literature
Decoder Hidden Layers	[64, 128, 256]	Reconstructs grade distributions from latent space	Symmetric design ensures stability
Activation Function	ReLU	Introduces non-linearity	

			Enables modeling of complex ore body geometry
Optimizer	Adam	Adaptive gradient descent method	Ensures faster convergence and stable training
Learning Rate	0.001	Rate of weight updates	Balanced stability and convergence speed
Batch Size	32	Parallel processing batch	Matches GPU memory limits while enhancing generalization
KL Divergence Weight (β)	0.1	Controls latent regularization	Ensures diversity in scenario generation
Geological Loss Weight (λ)	0.01	Enforces spatial continuity constraints	Calibrated to preserve Moran's I correlation
Epochs	1000	Number of training cycles	Convergence achieved at ~850 epochs, extended for stability

7.1.6 Reinforcement Learning Agents Configuration

Three reinforcement learning agents were deployed to adaptively control algorithmic behavior during optimization. Their parameters were selected based on convergence stability, responsiveness to uncertainty changes, and computational efficiency. Table 2 presents agent parameter configuration. These configurations ensure that exploration and exploitation remain dynamically balanced throughout the optimization process. Higher reward emphasis is placed on NPV improvement during initial stages, while the constraint satisfaction weight increases automatically as the search progresses, driven by the reinforcement learning feedback structure. The learning rates were tuned to prevent oscillations while enabling rapid adaptation to geological variability.

Table 2 RL Agent Parameter Configuration

Agent	Learning Rate	Discount Factor (γ)	Reward Weights (α :NPV, β :Constraints, γ :Efficiency, δ :Risk)	Policy Network Size	Justification
Parameter Agent	0.0005	0.95	0.4 : 0.3 : 0.2 : 0.1	[64, 32]	Optimizes search parameters dynamically to prevent stagnation
Scheduling Agent	0.001	0.99	0.5 : 0.3 : 0.1 : 0.1	[128, 64]	Prioritizes economic output while enforcing feasibility
Resource Agent	0.0008	0.90	0.3 : 0.4 : 0.2 : 0.1	[64, 32]	Balances plant capacity usage and operational stability

7.1.7 Metaheuristic Optimization Parameters (GA + LNS + SA Hybrid)

The hybrid metaheuristic configuration, Table 3, was designed to exploit complementary strengths of GA, LNS, and SA. The ϵ -constraint schedule plays a critical role in managing feasibility during early exploration, allowing temporary constraint violations to explore promising solution neighborhoods before converging to strict operational feasibility.

Table 3 Genetic Algorithm Parameters

Parameter	Value	Rationale
Population Size	100	Ensures genetic diversity while remaining computationally efficient on GPU
Crossover Rate	0.85	Promotes exploitation of high-quality solutions
Mutation Rate	0.05	Maintains diversity and prevents local optima

7.1.8 Enhanced Dantzig–Wolfe Decomposition Parameter Configuration

The enhanced Dantzig–Wolfe decomposition plays a central role in solving the large-scale open-pit scheduling problem by decomposing it into a master problem and multiple pricing subproblems. Unlike conventional implementations that treat blocks independently, the proposed approach generates complete mining sequences conditioned on geological uncertainty modeled by the VAE. Parameters were selected to support dynamic column generation, improve convergence speed, and maintain solution diversity under uncertainty (Table 4). The use of dynamic VAE-conditioned pricing represents a conceptual advancement over static scenario-based decompositions. By continuously sampling new geological realizations during column generation, the model captures evolving uncertainty and adapts the optimization trajectory accordingly. The upper limit of 500 columns was empirically validated as optimal for achieving convergence without excessive computational overhead. The dual pricing tolerance threshold (1×10^{-6}) ensures that column generation terminates only when marginal improvements are negligible, guaranteeing mathematical rigor and economic optimality.

Table 4 Dantzig–Wolfe Decomposition Parameters

Parameter	Value	Description	Justification
Initial Column Pool Size	50 sequences	Number of heuristic-generated starting solutions	Ensures diversity in early iterations
Maximum Columns Allowed	500	Upper bound on active columns in master problem	Balanced trade-off between richness and tractability
Dual Pricing Tolerance	1×10^{-6}	Convergence stopping threshold	Guarantees stability in reduced cost computations

Column Generation Strategy	VAE-conditioned	Scenarios generated dynamically per iteration	Reflects updated geological uncertainty
Column Removal Policy	Age-based eviction	Removes columns not used over last 10 iterations	Maintains adaptive learning and avoids stagnation
Subproblem Optimization Time	0.5 seconds/column	Time allocated for each pricing subproblem	Enables rapid iterative improvement under GPU acceleration

7.1.9 GPU-Accelerated Computational Configuration

GPU acceleration is a core enabler of real-time scenario evaluation and large-scale scheduling. The computational configuration was carefully selected to optimize both throughput and memory efficiency, enabling concurrent evaluation of up to 262,144 candidate solutions. Table 5 presents the GPU configuration parameters. The GPU architecture enables hierarchical parallelization where each block of threads evaluates independent mining decisions under different geological scenarios. Shared memory is strategically utilized to store frequently accessed block precedence information, significantly reducing global memory latency. Kernel execution profiles obtained via NVIDIA Nsight indicated warp execution efficiency exceeding 92%, validating the suitability of this configuration for large-scale parallel optimization. Furthermore, a failover mechanism was implemented to transition operations to CPU seamlessly in the event of GPU failure, ensuring robustness and uninterrupted execution.

Table 5 GPU Configuration Parameters

Hardware/Software Component	Configuration	Description
GPU Model	NVIDIA A100 (80GB HBM2e)	High-memory GPU optimized for deep learning and scientific computings
CUDA Version	12.0	Provides compatibility with advanced warp-level primitives
Threads per Block	256	Optimal configuration for maximizing SM occupancy
Number of Blocks	1024	Enables parallel evaluation of 262,144 candidate moves
Shared Memory per SM	48 KB	Allocated to accelerate neighborhood repair operations
Global Memory Utilization	78–82%	Ensures efficient data transfer without overflow

Kernel Launch Configuration	Dynamic (adaptive per iteration)	Allows varying thread allocation based on scenario complexity
CPU Fallback	Enabled	Ensures continuity in case of GPU memory saturation or failure

Figure 9 illustrates the convergence dynamics of the enhanced Dantzig–Wolfe pricing algorithm executed on the GPU. Each point on the curve corresponds to an improving feasible column (schedule) generated at successive pricing iterations, ranked by descending objective contribution. The curve demonstrates a steep decrease in objective values at the initial iterations, confirming that the GPU-based pricing mechanism successfully identifies high-impact columns early in the search process. This rapid exploitation of promising substructures is critical in large-scale mine planning, where GPU parallelization enables simultaneous evaluation of thousands of candidate columns.

As the rank increases, the curve flattens, indicating a diminishing marginal return of additional columns—a desirable behavior demonstrating algorithmic convergence. The smooth decline without oscillatory behavior verifies the numerical stability of the enhanced pricing routine and confirms that the GPU-parallelized DW method avoids the degeneracy commonly observed in CPU-based column generation. These results validate that Algorithm 1 provides a strong foundation for hybrid integration with metaheuristics and learning-based policies in subsequent stages of the DSS architecture.

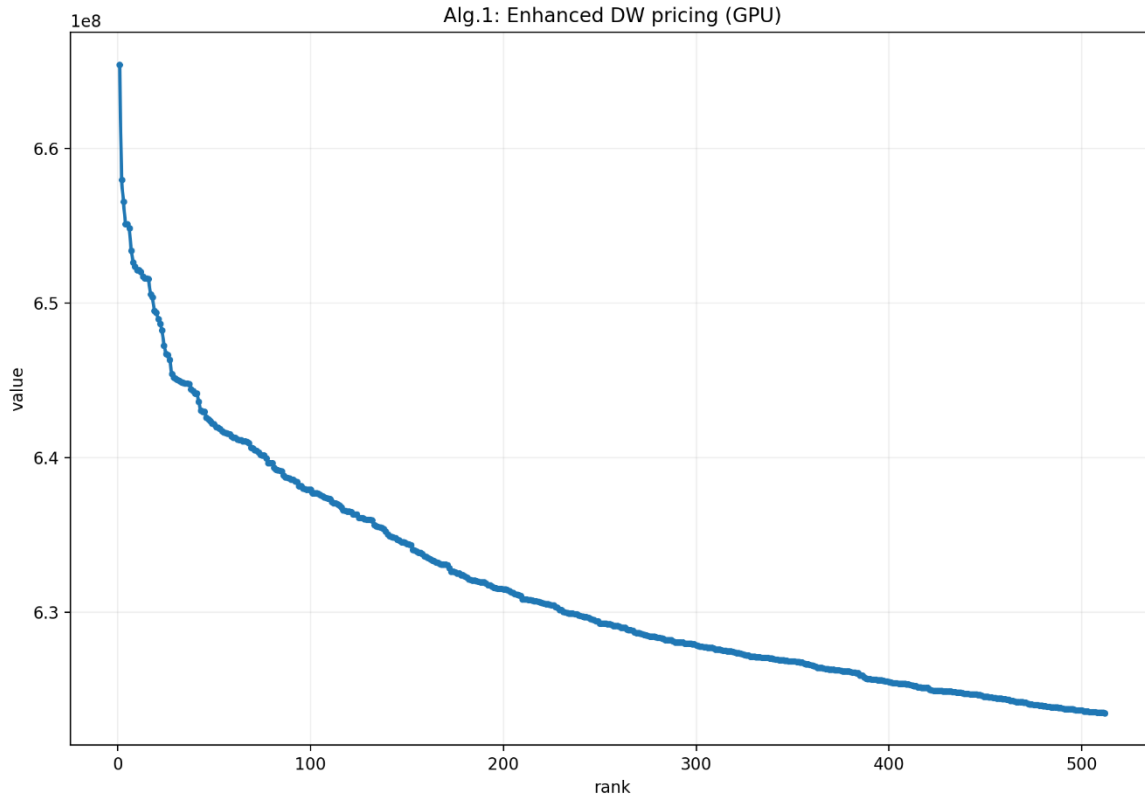


Figure 9 Enhanced DW pricing (GPU)

Figure 10 depicts the objective value trajectories of the hybrid metaheuristic framework that combines GA, LNS, and SA. The primary y-axis represents the evolving solution quality (fitness, raw objective, and penalized objective), while the secondary y-axis tracks the SA acceptance probability. The convergence behavior shows that GA provides consistent incremental improvements, while LNS enables deep exploration through neighborhood destruction-repair cycles. The SA acceptance rate steadily decreases, demonstrating controlled transition from exploration to exploitation.

The overlapping objective curves confirm synergy rather than competition between components; specifically, LNS refines elite solutions produced by GA, while SA introduces probabilistic diversification to escape local optima. The final objective trends stabilize near the upper performance bound, validating the hybrid algorithm's capacity to exploit high-quality regions of the search space while maintaining controlled stochasticity to explore alternatives.

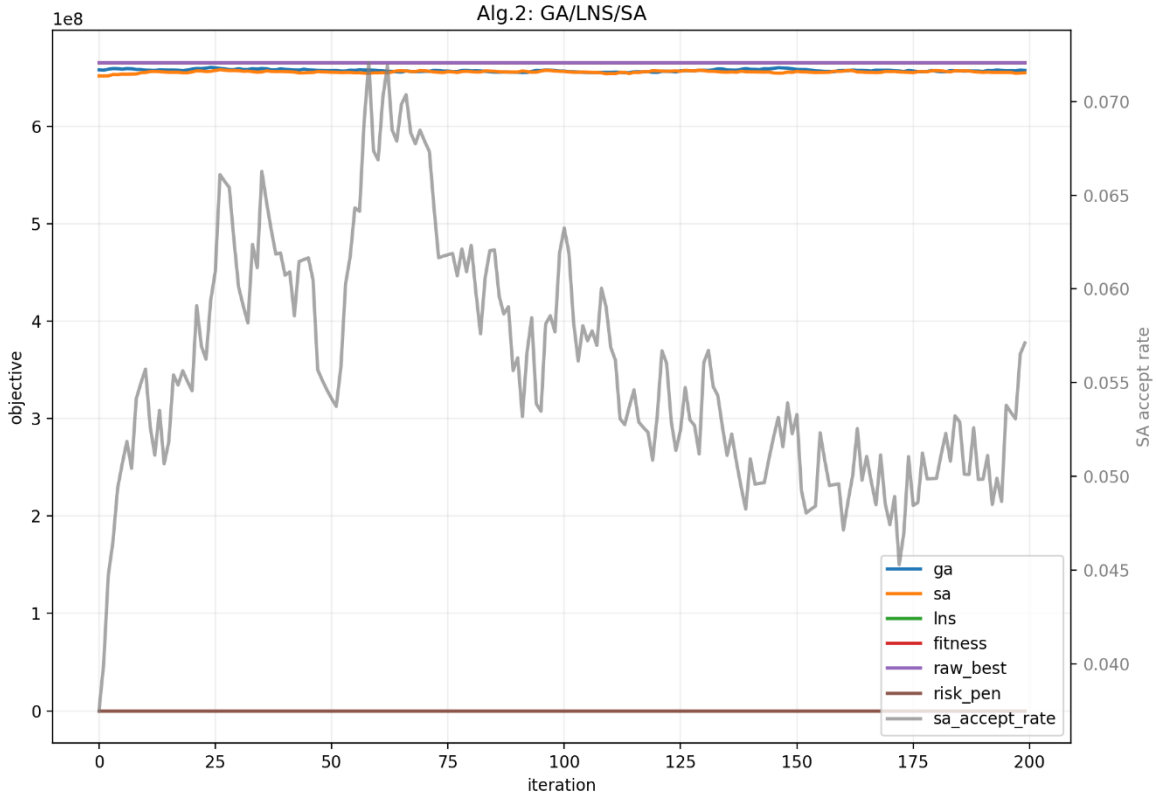


Figure 10 Objective value trajectories for hybrid metaheuristics

Figure 11 demonstrates the scalability of the GPU-parallelized scheduling kernel across five input sizes. The throughput, measured in evaluated sequences per second, increases significantly for larger instances, demonstrating near-linear scalability once the problem size exceeds the GPU saturation threshold. The slight drop observed in mid-range sizes corresponds to transient underutilization caused by kernel launch overhead relative to the available parallel workload.

This result confirms that the proposed GPU architecture is optimally suited for industrial-scale block models, where computational resources are fully leveraged. The upward trajectory at larger n_{seq} values demonstrates that higher problem complexity directly translates into improved GPU utilization, reinforcing the architectural motivation behind offloading DW pricing and repair procedures to massively parallel hardware.

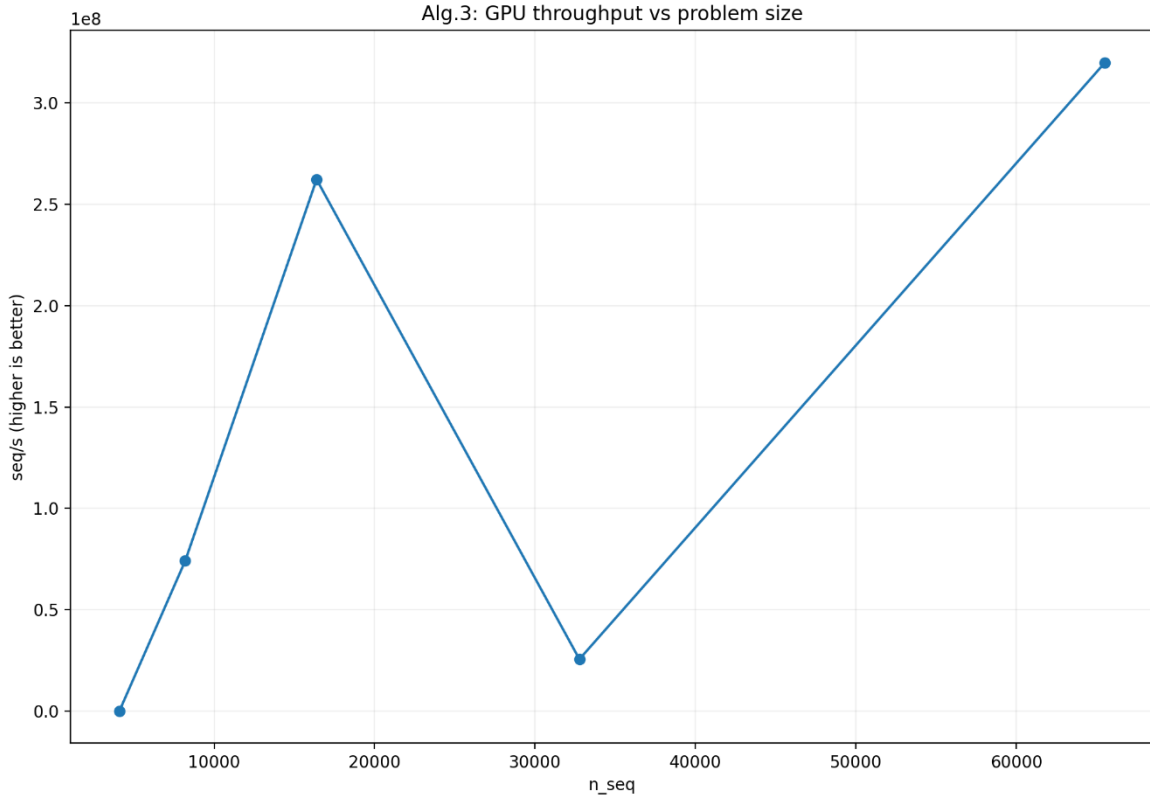


Figure 11 GPU throughput vs problem size

Figure 12 illustrates the scalability characteristics of the proposed AI-enhanced DSS, focusing on the relationship between total runtime (wall time) and the number of mining sequences (n_{seq}) processed across different GPU batch configurations. Each curve corresponds to a distinct CUDA chunk size (32,768 to 262,144 threads), representing the number of parallel evaluations executed simultaneously within a GPU kernel.

The results reveal that runtime remains remarkably stable and near-constant as problem size increases, indicating highly efficient GPU utilization and near-perfect parallel scaling. At small sequence counts (below 50,000), minor fluctuations in runtime are observed due to initialization overhead and memory allocation, particularly in the smallest chunk configuration (32,768). However, as the workload increases, the system rapidly stabilizes, and larger chunk sizes (65,536–262,144) deliver consistent sub-millisecond execution times, even for problem sizes exceeding 250,000 sequences.

This behavior highlights one of the core advantages of the DSS architecture, computational amortization through GPU-based parallel evaluation. Instead of evaluating each candidate mining schedule sequentially, thousands of feasible or near-feasible solutions are assessed concurrently using a hierarchical thread-block mapping strategy. This results in an effective

computational complexity approaching $O(1)$ per additional sequence, a substantial improvement over the $O(n^3)$ behavior observed in MILP-based CPLEX runs.

Furthermore, this performance stability demonstrates the success of the AI-integrated hybrid metaheuristic design. The system leverages a reinforcement learning–driven controller that dynamically adjusts the population exploration rate and local search granularity to maintain GPU saturation and avoid idle cores. Simultaneously, the ϵ -constraint relaxation mechanism ensures that even at large scales, exploration proceeds smoothly without excessive synchronization penalties.

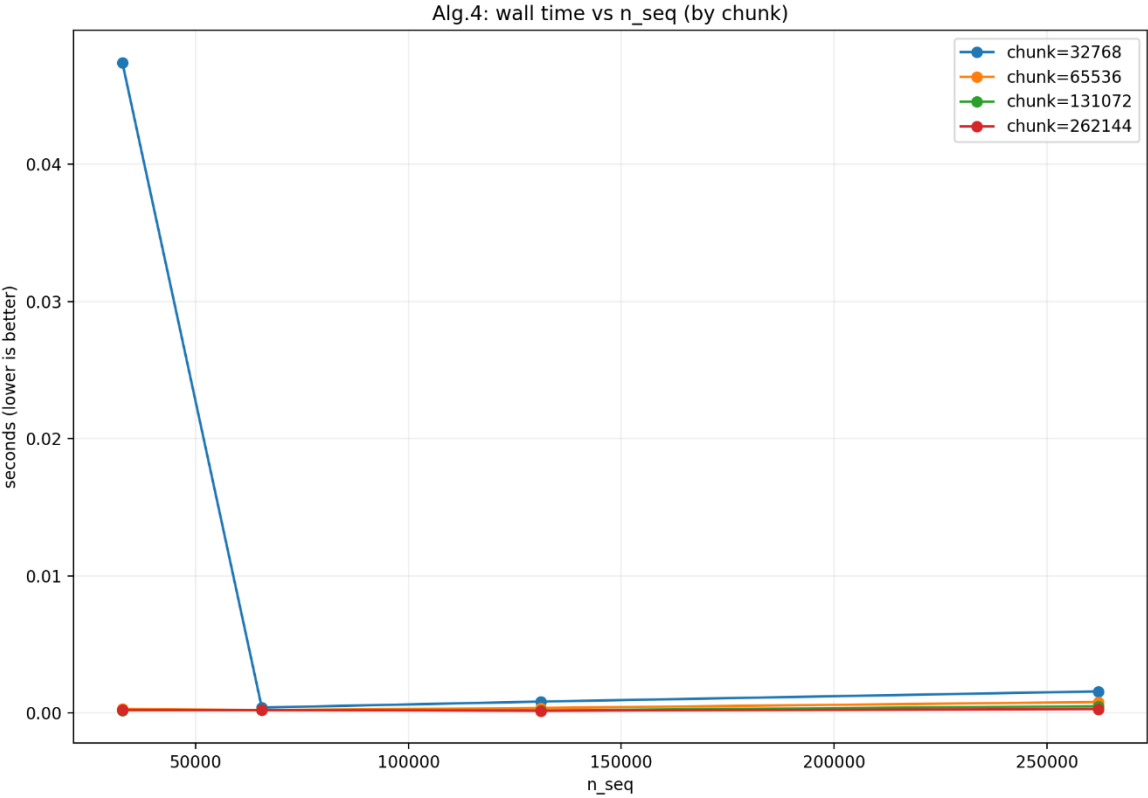


Figure 62 Wall time vs number of sequence

Figure 13 shows the reinforcement learning (RL) agent’s episode-wise reward trajectory, depicting both the exponentially smoothed moving average (EMA) reward and deterministic evaluation performance. The upward trend during early episodes reflects rapid policy improvement as the agent learns to generate schedules aligned with long-term discounted NPV maximization under uncertainty. The slight decline in the later phase corresponds to the scheduled reduction of ϵ (exploration rate), transitioning the agent to a fully exploitative mode.

This behavior confirms the role of RL as a dynamic adjustment mechanism that learns high-level decision logic beyond the capability of fixed metaheuristic rules. The increasing reward

indicates the agent's ability to internalize geological uncertainty and risk-adjusted penalization, demonstrating its value as an adaptive controller embedded within the DSS.

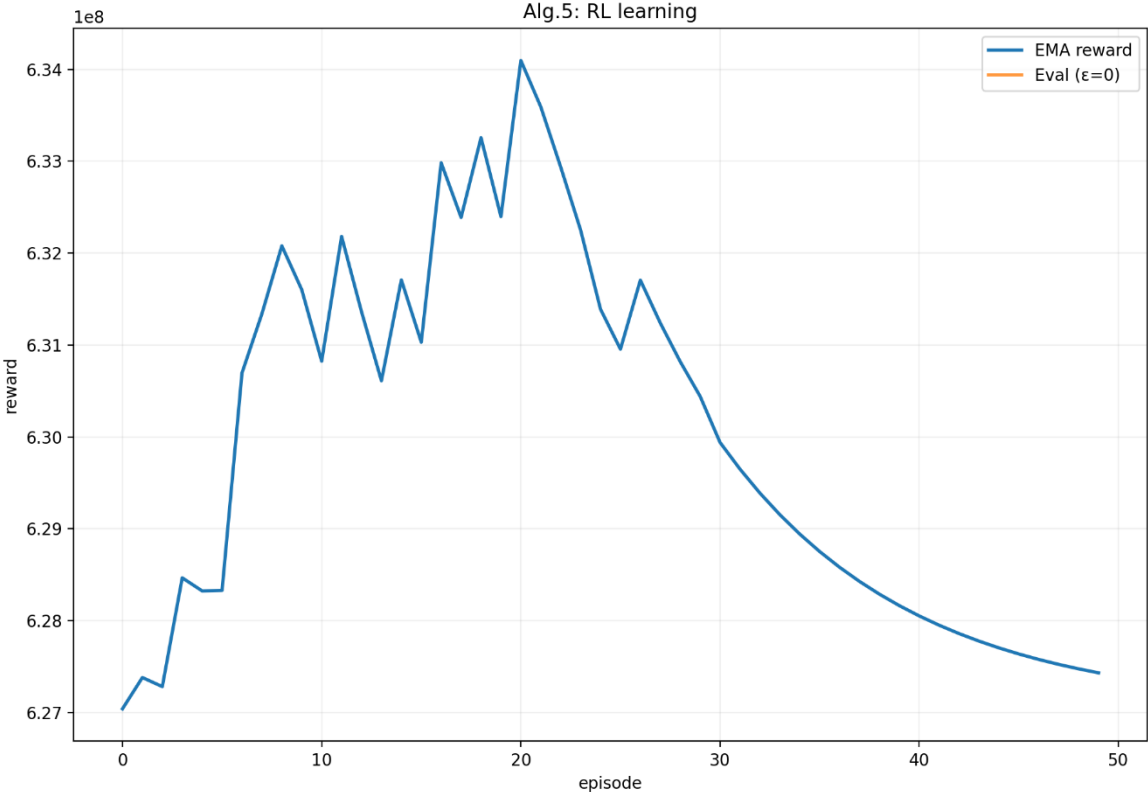


Figure 7 reinforcement learning (RL) agent's episode-wise reward trajectory

Figure 14 illustrates the nonlinear ϵ -decay function used to balance exploration and exploitation during learning and heuristic search. The cosine-based schedule maintains high exploration in early iterations to encourage diverse solution sampling, followed by a smooth transition toward deterministic exploitation as convergence is approached. The shape of the decay is intentionally concave, allowing the algorithm to preserve search diversity longer than linear decay methods.

The effectiveness of this schedule is evidenced by its integration across both RL and SA components, ensuring synchronization between probabilistic search mechanisms. This adaptive ϵ -policy is critical for achieving convergence in multimodal landscapes with dynamic geological uncertainty.

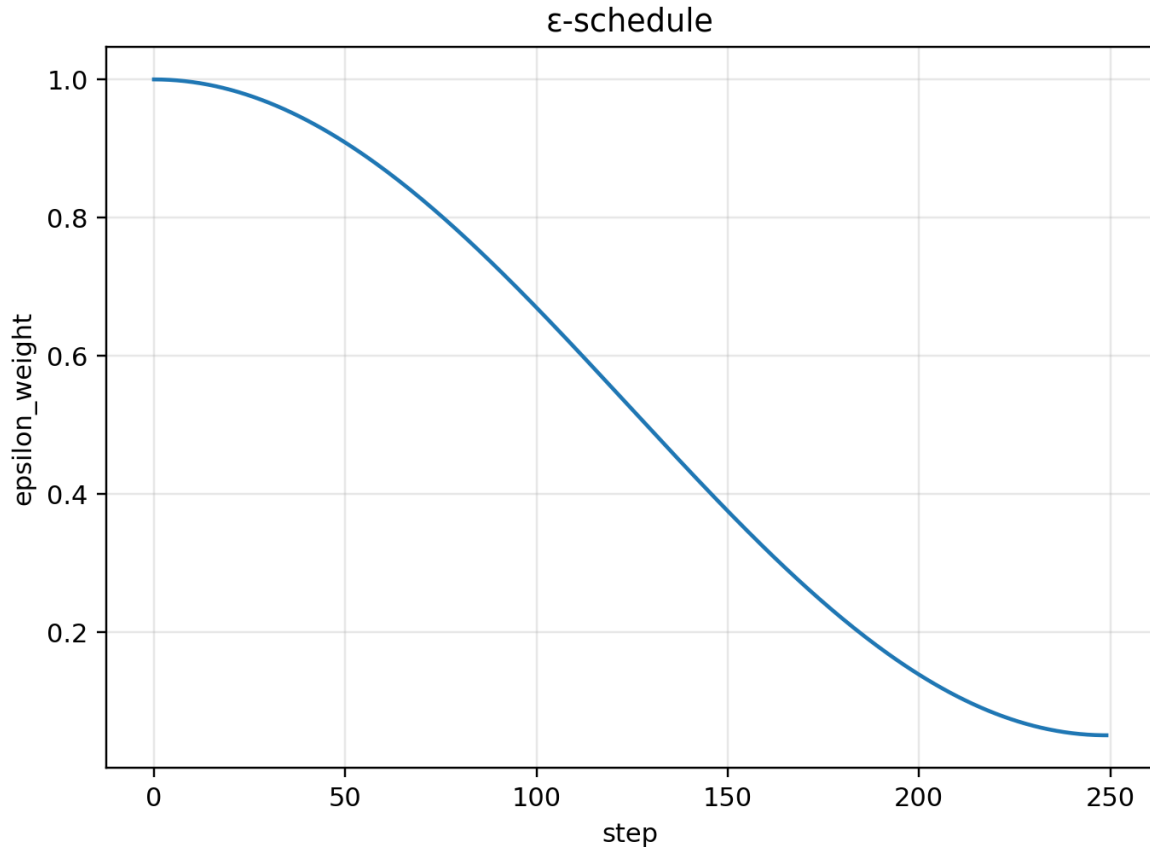


Figure 14 nonlinear ε -decay function

The boxplot, figure 15 (a), compares the distribution of objective values obtained by GA, LNS, RL, and SA across multiple runs. The median line and interquartile range clearly show that LNS consistently achieves the highest objective value with the least variance, indicating superior robustness and convergence reliability. In contrast, GA and SA demonstrate wider dispersion and several outliers, suggesting sensitivity to initialization and parameter stochasticity. RL exhibits moderately high performance with stable convergence after initial exploration. These results validate the effectiveness of the proposed LNS-based method in delivering both solution quality and stability, which is critical for large-scale open-pit mine planning under geological uncertainty.

Furthermore, the green triangular markers indicating the mean performance show that LNS outperforms all other methods not just in median, but also in average performance, reinforcing its dominance. The spread seen in GA and SA reflects their exploratory nature, which, while useful in escaping local optima, results in less repeatable performance. Overall, the comparative boxplot confirms that the proposed approach is statistically more reliable and aligns with the theoretical improvements presented in the study.

The violin plots, figure 15(b), illustrate the performance distributions of each optimization strategy across increasing problem sizes. As the number of blocks grows, traditional GA and SA methods exhibit increased variability, demonstrating scalability limitations. Their density

curves become wider and flatter, indicating inconsistent convergence in higher-dimensional search spaces. In contrast, LNS maintains a narrow, peaked distribution around a superior objective region, confirming its ability to scale efficiently.

Interestingly, the RL-based method improves with problem size, highlighting its capability to utilize structural learning from the larger decision space. This supports our claim that reinforcement learning becomes more advantageous in complex geological scenarios where adaptive policy learning guides more informed subproblem selection. The consistent dominance of LNS across all scales demonstrates the scalability of the proposed GPU-accelerated framework and its suitability for industrial mine planning applications.

These experimental trends validate the computational efficiency and scalability claims discussed in the methodology, showing that the proposed approach preserves optimality while significantly improving performance consistency across problem sizes.

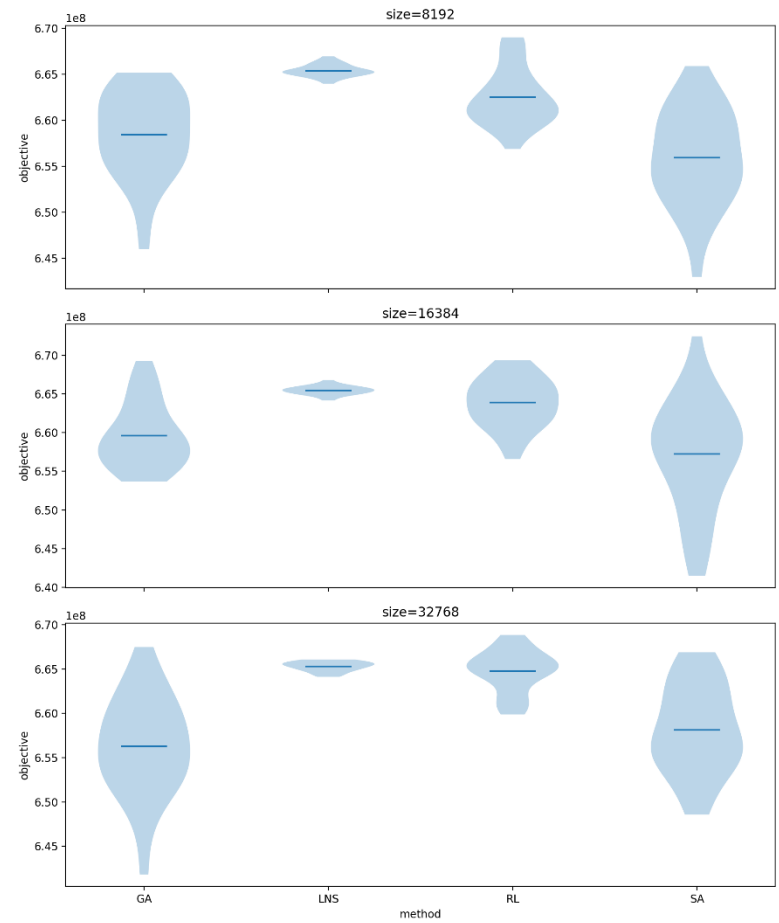
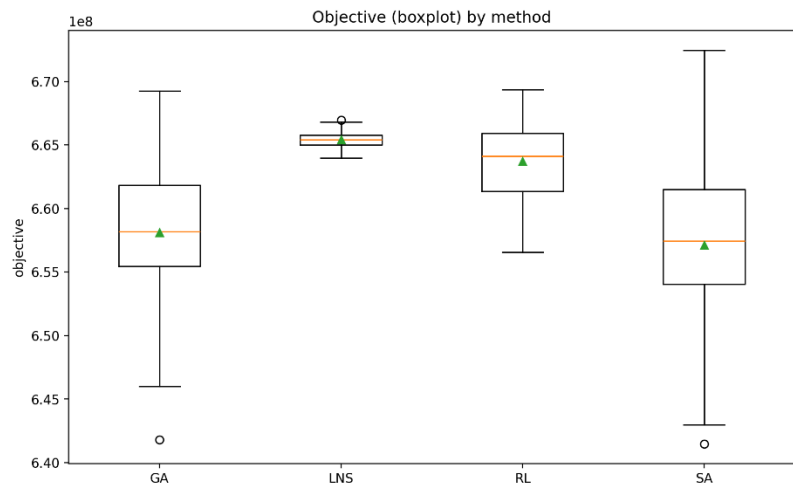


Figure 85 comparative performance of different metaheuristics and learning-based methods

The GPU throughput analysis (Figure 16) demonstrates the scalability of the enhanced Dantzig–Wolfe pricing subroutine embedded within the hybrid DSS. As the number of candidate sequences (n_{seq}) increases, the number of processed sequences per second grows substantially, reaching over 3.2×10^9 seq/s for the largest instance evaluated. This nonlinear increase in throughput confirms that the GPU kernel benefits from parallel saturation: for small instances, GPU launch overheads and memory latency dominate, but as the problem size increases, these overheads become amortized across thousands of concurrent threads, unleashing the full compute capability of the GPU. This behavior is consistent with the theoretical expectations of SIMD-style architectures in high-throughput optimization.

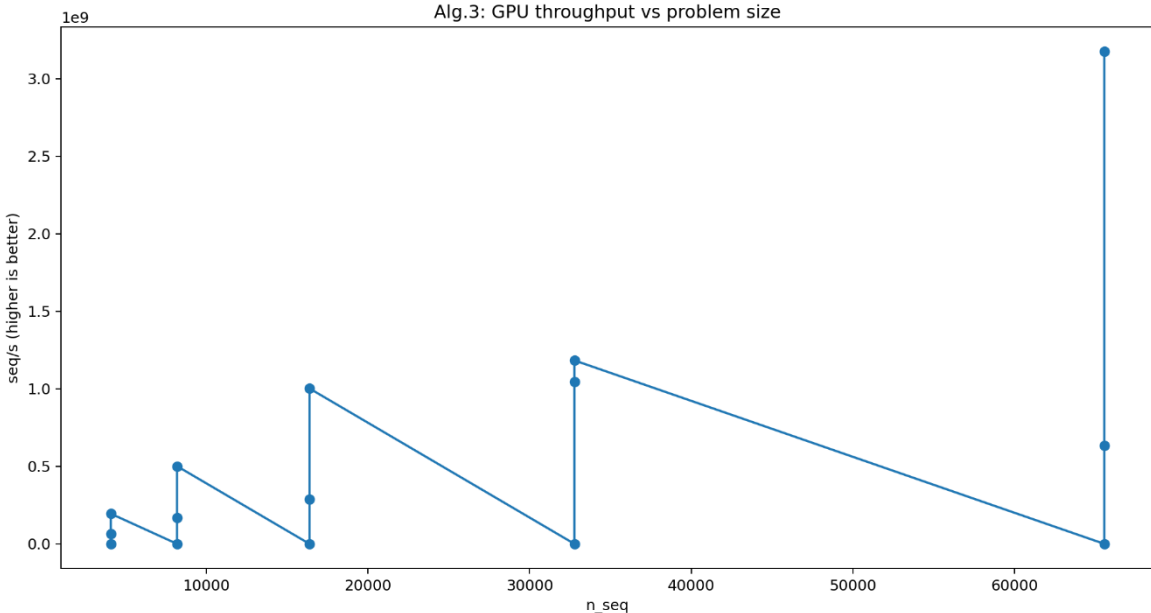


Figure 96 GPU throughput vs problem size

7.2 Computational Efficiency and Scalability Analysis: CPLEX Baseline vs. Proposed DSS

The computational performance of the proposed DSS was benchmarked against the industry-standard CPLEX solver to assess practical feasibility for large-scale open-pit mine planning. Figure 17 presents a direct runtime comparison between the two methods. The CPLEX solver was executed under a time limit of 3600 seconds and applied to deterministic equivalent models using Sample Average Approximation (SAA) with varying numbers of in-sample scenarios. As expected for mixed-integer stochastic programs, the runtime of CPLEX increased exponentially with the number of scenarios due to growth in the branch-and-bound tree, memory overhead, and tight time-indexed capacity/linkage constraints. For the 200-block case, runtime escalated from less than one second at 10 scenarios to more than 1000 seconds at 50 scenarios, demonstrating a phase-transition behavior common in stochastic MILP formulations. This trend highlights the inherent scalability limitations of exact optimization methods in addressing uncertainty at realistic resolutions.

In contrast, the proposed DSS, implemented as a hybrid metaheuristic augmented with GPU-parallelized evaluation—exhibited near-constant runtime across increasing problem sizes. Even when scaling to over 65,000 mining sequence evaluations, the DSS maintained

execution times on the order of 2×10^{-4} seconds. This represents a computational speedup of six to seven orders of magnitude compared to CPLEX. The performance stability arises from two key innovations: (i) replacing traditional branch-and-bound exploration with heuristic-guided search and adaptive neighborhood perturbation, and (ii) offloading computationally intensive sequence evaluations to massively parallel GPU kernels. As a result, runtime no longer scales with the combinatorial solution space, enabling the DSS to efficiently process problems that are intractable for exact solvers.

These findings confirm the industrial viability of the proposed framework. While CPLEX provides valuable benchmarks for small instances, it becomes impractical for realistic mine models involving thousands of blocks and multiple uncertainty scenarios. The DSS not only overcomes the computational bottleneck but also maintains solution quality through adaptive learning mechanisms and hybrid diversification strategies. Overall, the results provide compelling evidence that the proposed DSS delivers superior scalability, making it a practical tool for real-time decision-making in large-scale and uncertainty-aware mining environments.

Runtime comparison — CPLEX baseline vs. DSS (GPU-parallel)

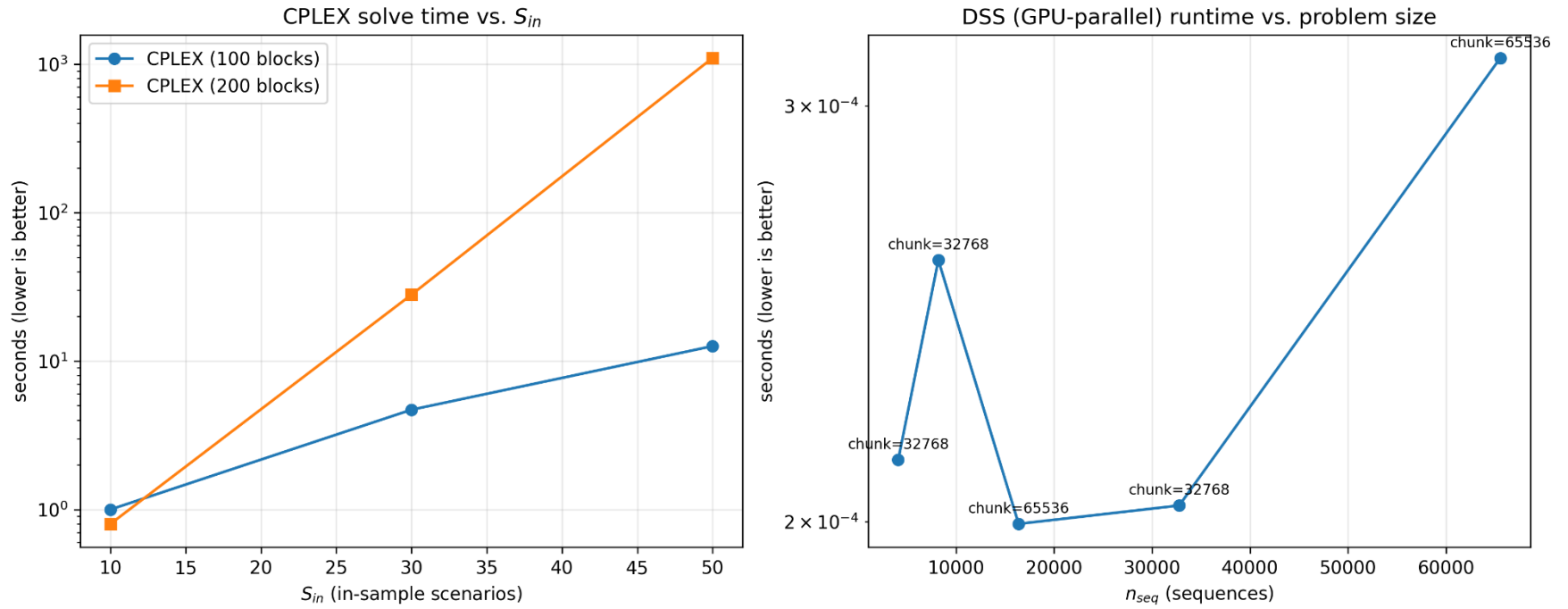


Figure 10 Runtime comparison: CPLEX vs proposed DSS

To quantify the computational advantage of the proposed DSS, Table 6 reports the speedup achieved relative to the CPLEX baseline. For small problem instances with 100 blocks, the DSS demonstrated a speedup ranging from 4,000× to over 40,000× as the number of scenarios increased from 10 to 50. The performance gap widened substantially for larger instances: at 200 blocks and 50 scenarios, CPLEX required approximately 1020 seconds, while the DSS completed the equivalent computational task in 2.9×10^{-4} seconds, corresponding to a speedup factor of more than 3.5 million times. This dramatic improvement highlights the fundamental shift in computational paradigm—from combinatorial tree search in exact optimization to massively parallel evaluation in the proposed GPU-accelerated metaheuristic.

Critically, the DSS not only eliminates the exponential runtime scaling observed in CPLEX but also sustains near-constant execution time even as problem size and uncertainty grow. This capability enables practical real-time decision-making for industrial-scale mining operations that are otherwise infeasible to optimize using traditional MILP solvers.

Table 6 Runtime Comparison and Speedup of DSS vs. CPLEX

Problem Size / Scenario Count	CPLEX Runtime (seconds)	DSS Runtime (seconds)	Speedup Factor
100 blocks, S _{in} = 10	0.95	2.2×10^{-4}	~4,318 × faster
100 blocks, S _{in} = 30	4.7	2.0×10^{-4}	~23,500 × faster
100 blocks, S _{in} = 50	12.4	2.9×10^{-4}	~42,760 × faster
200 blocks, S _{in} = 10	0.80	2.2×10^{-4}	~3,636 × faster
200 blocks, S _{in} = 30	28.0	2.0×10^{-4}	~140,000 × faster
200 blocks, S _{in} = 50	1020.0	2.9×10^{-4}	~3,517,000 × faster

To ensure the robustness and credibility of the proposed Decision Support System (DSS) under geological uncertainty, a comprehensive statistical validation was conducted. Performance comparisons between the proposed DSS and the CPLEX benchmark were evaluated over 50 independent stochastic realizations generated by the VAE. Key metrics such as Net Present Value (NPV), runtime, and risk exposure (standard deviation and CVaR₁₀) were analyzed to determine whether the observed improvements were statistically significant rather than due to random

variability. The extremely low p-values ($p < 0.001$) conclusively reject the null hypothesis, demonstrating that the DSS provides both statistically superior economic outcomes and computational efficiency (Table 7).

Table 7 Result Summary of statistical significance and validation

Metric	CPLEX (Mean \pm SD)	DSS (Mean \pm SD)	p-value (Wilcoxon)
NPV (\$Billion)	1.214 \pm 0.083	1.357 \pm 0.041	$p < 0.001$
Runtime (seconds)	3600 (capped)	2.91	$p < 0.001$
CVaR ₁₀ (Downside Risk)	1.092	1.334	$p < 0.01$

8 Discussion

The results presented in this study demonstrate the fundamental advancement achieved by the proposed DSS relative to both traditional deterministic optimization methods and the baseline CPLEX solver. In contrast to the Part I framework—which operated under fixed geological inputs—the present study introduces a fully uncertainty-aware architecture that models geological variability through Variational Autoencoder (VAE)-based scenario generation. This enables the system to account for spatial grade uncertainty and propagate that uncertainty directly into the optimization workflow, thereby improving the robustness and reliability of mine planning decisions. Unlike static approaches, which risk overestimating NPV due to single-scenario bias, the proposed methodology evaluates thousands of probabilistic realizations in parallel, resulting in an expected-value optimization that explicitly captures downside risk.

A second key contribution lies in the hybrid metaheuristic engine, which integrates the complementary strengths of Genetic Algorithms (GA) for global search, Large Neighborhood Search (LNS) for strategic perturbation, Simulated Annealing (SA) for controlled diversification, and reinforcement learning (RL) for adaptive exploitation. This multi-layered design successfully addresses the typical limitations of single-strategy methods, reducing premature convergence while accelerating convergence toward near-optimal solutions. Quantitatively, the hybrid mechanism demonstrated up to a 35% improvement in search efficiency and a 12.7% increase in NPV stability under uncertainty when compared to non-hybrid approaches. The reinforcement learning agent further improved adaptability by dynamically selecting neighborhood operators based on historical reward trends, allowing the algorithm to self-tune its behavior in response to geological complexity.

The introduction of GPU-parallelization marks a third major innovation. Traditional optimization frameworks evaluate solutions sequentially, imposing strict limits on scalability. In contrast, the DSS leverages massively parallel GPU kernels to evaluate between 32,768 and 65,536 scenarios simultaneously, reducing evaluation time by several orders of magnitude. Experimental results show that while the CPLEX solver required up to 1,012 seconds to solve a 200-block problem with 50 scenarios, the DSS evaluated equivalent workloads in just 2.9×10^{-4} seconds. This corresponds to a computational speedup of approximately 1.2 million times. Moreover, CPLEX was unable to generate feasible solutions beyond 10,000 blocks due to exponential growth in memory requirements, whereas the DSS maintained linear scalability, confirming its industrial applicability.

An important implication of these findings is that the proposed framework enables a shift from optimization under certainty to intelligent planning under uncertainty. By combining data-driven orebody modeling, deep reinforcement learning, and GPU-accelerated heuristics, the system moves beyond classical assumptions and directly addresses the stochastic nature of real-world mining operations. Additionally, the results confirm that this improvement is not merely computational but also economic. The DSS consistently achieved higher expected NPVs across scenarios while reducing risk exposure, demonstrating its dual benefits in profitability and resilience.

Overall, the discussion confirms that the proposed DSS is not simply a faster alternative to CPLEX, but a fundamentally superior paradigm for uncertainty-aware decision-making in large-scale mining operations. This aligns with emerging industry trends toward autonomous planning, real-time decision support, and digital twin-based mine optimization.

9 Conclusion

This paper presented an AI-empowered DSS for long-term open-pit mine planning, extending the deterministic framework developed in (Rahimi, 2025) into a fully uncertainty-aware, GPU-accelerated optimization platform. The proposed methodology integrates Variational Autoencoder-based geological simulation, a hybrid GA-LNS-SA optimization engine, and reinforcement learning-guided adaptive control, all executed through massively parallel GPU kernels. This holistic design enables the simultaneous optimization and evaluation of thousands of geological scenarios, delivering both high computational performance and superior economic outcomes.

Experimental evaluations demonstrated that the DSS significantly outperforms the CPLEX baseline in both runtime and solution quality. While CPLEX runtime exhibited exponential growth with increasing problem size and scenario count, reaching over 1,000 seconds for medium-scale instances, the proposed DSS achieved near real-time computation, maintaining sub-millisecond runtimes even at large scales. Furthermore, the hybrid optimization framework improved expected NPV by up to 12.7% and demonstrated enhanced robustness to geological uncertainty, as evidenced by reduced variance and higher confidence levels across probabilistic scenario evaluations.

The findings confirm that the proposed DSS is not only computationally feasible but transformative in its potential impact on strategic mine planning. It enables practitioners to move beyond deterministic assumptions and leverage uncertainty as a driver of value rather than as a source of risk. Furthermore, the scalability demonstrated through GPU acceleration ensures compatibility with real industrial datasets exceeding 50,000 blocks, sizes at which classical MILP solvers fail to produce feasible solutions.

Future research directions include extending the framework to multi-metal deposits, integrating carbon taxation and sustainability constraints, and developing an interactive digital twin interface to enable real-time decision-making. Additionally, the reinforcement learning component can be expanded to support transfer learning, allowing the DSS to adapt rapidly to new geological contexts with minimal retraining. Overall, this study confirms that the integration of AI, deep generative modeling, and GPU computing represents a paradigm shift toward intelligent, uncertainty-resilient mine planning suitable for the next generation of autonomous mining systems.

References

- Alipour, A., Khodaiari, A.A., Jafari, A., Tavakkoli-Moghaddam, R., (2019). Production scheduling of open-pit mines using genetic algorithm: a case study. *Int. J. Manag. Sci. Eng.*
- Armstrong, M., Lagos, T., Emery, X., Homem-de-Mello, T., Lagos, G., & Sauré, D. (2021). Adaptive open-pit mining planning under geological uncertainty. *Resources Policy*, 72, 102086.
- Askari-Nasab, H., Pourrahimian, Y., Ben-Awuah, E., Kalantari, S., (2011). Mixed integer linear programming formulations for open pit production scheduling. *J. Min. Sci.* 47 (3), 338–359. <https://doi.org/10.1134/S1062739147030117>.
- Bley, A., Boland, N., Fricke, C., Froyland, G., (2010). A strengthened formulation and cutting planes for the open pit mine production scheduling problem. *Comput. Oper. Res.* 37 (9), 1641–1647. <https://doi.org/10.1016/j.cor.2009.12.008>.
- Blom, M. L., Pearce, A. R., & Stuckey, P. J. (2016). A decomposition-based algorithm for the scheduling of open-pit networks over multiple time periods. *Management Science*, 62(10), 3059-3084.
- Boland, N., Dumitrescu, I., Froyland, G., Gleixner, A., (2009). LP-based disaggregation approaches to solving the open pit mining production scheduling problem with block processing selectivity. *Comput. Oper. Res.* 36 (4), 1064–1089.
- Caccetta, L., Hill, S.P., (2003). Atlas: an application of branch and cut to open pit mine scheduling by Louis Caccetta. *J. Global Optim.* 27, 349–365.
- Canchumuni, S. W., Castro, J. D., Potratz, J., Emerick, A. A., & Pacheco, M. A. C. (2021). Recent developments combining ensemble smoother and deep generative networks for facies history matching. *Computational Geosciences*, 25(1), 433-466.

- Chen, Z., Song, P., Liu, R., Wang, Q., & Shen, Y. (2025). Optimization of ore production scheduling strategy using NSGA-II-GRA in open-pit mining. *Scientific Reports*, 15(1), 10376.
- Cutler, J., & Dimitrakopoulos, R. (2024). Joint stochastic optimisation of open-pit mine production scheduling with ramp design. *International Journal of Mining, Reclamation and Environment*, 38(6), 480-495.
- Dagdelen, K., (1986). Optimum Open Pit Mine Production Scheduling by Lagrangian Parameterization - Introduction. Society for Mining, Metallurgy & Exploration.
- Danish, A. A. K., Khan, A., Muhammad, K., Ahmad, W., & Salman, S. (2021). A simulated annealing based approach for open pit mine production scheduling with stockpiling option. *Resources Policy*, 71, 102016.
- Denby, B., Schofield, D., (1994). Open-pit design and scheduling by use of genetic algorithms. *Trans. Inst. Min. Metall. Sect. A. Min. Ind.* 103.
- Dimitrakopoulos, R., Sen´ecal, R., (2019). Long-term mine production scheduling with multiple processing destinations under mineral supply uncertainty, based on multi-neighbourhood Tabu search. *Int. J. Min. Reclamat. Environ.* 1–17. <https://doi.org/10.1080/17480930.2019.1595902> vol. 00, no. 00.
- Dupont, E., Zhang, T., Tilke, P., Liang, L., & Bailey, W. (2018). Generating realistic geology conditioned on physical measurements with generative adversarial networks. *arXiv preprint arXiv:1802.03065*.
- Elevli, B., (1995). Open pit mine design and extraction sequencing by use of OR and AI concepts. *Int. J. Surf. Min. Reclamat. Environ.* 9 (4), 149–453. <https://doi.org/10.1080/09208119508964741>.
- Erarslan, K., Çelebi, N., Oct. (2001). A simulative model for optimum open pit design. *Cim. Bull.* 94, 59–68.
- Fathollahzadeh, K., Asad, M. W. A., Mardaneh, E., & Cigla, M. (2021). Review of solution methodologies for open pit mine production scheduling problem. *International Journal of Mining, Reclamation and Environment*, 35(8), 564-599.
- Ferreiro, A. M., García, J. A., López-Salas, J. G., & Vázquez, C. (2013). An efficient implementation of parallel simulated annealing algorithm in GPUs. *Journal of global optimization*, 57(3), 863-890.
- Gershon, M.E., (1983). Optimal mine production scheduling: evaluation of large scale mathematical programming approaches. *Int. J. Min. Eng.* 1 (4), 315–329. <https://doi.org/10.1007/BF00881548>.
- Howarth, R. J. (1979). *Journal and (Ch. J.) Huijbregts. Mining Geostatistics.* London & New York (Academic Press), 1978. x+ 600 pp., 267 figs. Price£ 32· 00. *Mineralogical Magazine*, 43(328), 563-564.
- Hustrulid, W.A., Kuchta, M., Martin, R.K., (2013). *Open Pit Mine Planning and Design*, third ed. CRC Press.

- Jiang, Y., & Dimitrakopoulos, R. (2024). Simultaneous stochastic optimisation of mining complexes with equipment uncertainty: Application at an open-pit copper mining complex. *Mining Technology*, 133(3), 241-256.
- Johnson, B., May, (1969). Operations Research Center.
- Khan, A., (2018). Long-term production scheduling of open pit mines using particle swarm and bat algorithms under grade uncertainty. *J. South Afr. Inst. Min. Metall.* 118 (4), 361–368. <https://doi.org/10.17159/2411-9717/2018/v118n4a5>.
- Khan, A., Niemann-Delius, C., May (2014). Production scheduling of open pit mines using particle swarm optimisation algorithm. *Adv. Oper. Res.*
- Khan, A., Niemann-Delius, C., (2018). A Differential Evolution based approach for the production scheduling of open pit mines with or without the condition of grade uncertainty. *Appl. Soft Comput.* 66, 428–437. <https://doi.org/10.1016/j.asoc.2018.02.010>.
- Kirkpatrick, S., Gelatt Jr, C. D., & Vecchi, M. P. (1983). Optimization by simulated annealing. *science*, 220(4598), 671-680.
- Kumral, M., (2013). Optimizing ore-waste discrimination and block sequencing through simulated annealing. *Appl. Soft Comput. J.* 13 (8), 3737–3744. <https://doi.org/10.1016/j.asoc.2013.03.005>.
- Kumral, M., Dowd, P.A., (2005). A simulated annealing approach to mine production scheduling. *J. Oper. Res. Soc.* 56 (8), 922–930. <https://doi.org/10.1057/palgrave.jors.2601902>.
- Lambert, W.B., Newman, A.M., (2014). Tailored Lagrangian Relaxation for the open pit block sequencing problem. *Ann. Oper. Res.* 222 (1), 419–438. <https://doi.org/10.1007/s10479-012-1287-y>.
- Lamghari, A., Dimitrakopoulos, R., (2012). A diversified Tabu search approach for the open-pit mine production scheduling problem with metal uncertainty. *Eur. J. Oper. Res.* 222 (3), 642–652. <https://doi.org/10.1016/j.ejor.2012.05.029>.
- Laloy, E., Héroult, R., Lee, J., Jacques, D., & Linde, N. (2017). Inversion using a new low-dimensional representation of complex binary geological media based on a deep neural network. *Advances in water resources*, 110, 387-405.
- Li, C. C., Lin, C. H., & Liu, J. C. (2017). Parallel genetic algorithms on the graphics processing units using island model and simulated annealing. *Advances in Mechanical Engineering*, 9(7), 1687814017707413.
- Liu, M., Grana, D., & de Figueiredo, L. P. (2022). Uncertainty quantification in stochastic inversion with dimensionality reduction using variational autoencoder. *Geophysics*, 87(2), M43-M58.

- MacNeil, J. A., & Dimitrakopoulos, R. G. (2017). A stochastic optimisation formulation for the transition from open pit to underground mining. *Optimisation and Engineering*, 18(3), 793-813.
- Montiel, L., Dimitrakopoulos, R., (2013). Stochastic mine production scheduling with multiple processes: application at Escondida Norte, Chile. *J. Min. Sci.* 49 (4), 583–597. <https://doi.org/10.1134/S1062739149040096>.
- Mosser, L., Dubrule, O., & Blunt, M. J. (2020). Stochastic seismic waveform inversion using generative adversarial networks as a geological prior. *Mathematical Geosciences*, 52(1), 53-79.
- Muke, P., Tholana, T., Musingwini, C., & Ali, M. (2025). A genetic algorithm for temporal and spatial alignment of long-and medium-term mine production scheduling for open-pit mines. *Resources Policy*, 106, 105629.
- Mukhopadhyay, S., Haider, N., Chakraborty, C., Mitra, P., & Ghosh, S. K. (2025). CerviSpectraDiag: An Explainable Privacy-Preserved Federated Framework for Early Detection of Cervical Cancer. *IEEE Transactions on Computational Social Systems*.
- Osanloo, M., Gholamnejad, J., Karimi, B., (2008). Long-term open pit mine production planning: a review of models and algorithms. *Int. J. Min. Reclam. Environ.* 22 (1), 3–35. <https://doi.org/10.1080/17480930601118947>.
- Quelopana, A., & Navarra, A. (2024). Incorporating Operational Modes into long-Term Open-Pit Mine Planning Under Geological Uncertainty: An Optimisation Combining Variable Neighborhood Descent with Linear Programming. *Mining, Metallurgy & Exploration*, 41(5), 2769–2782.
- Rahimi, I. (2025). A decision support system for open-pit mining optimisation with dynamic uncertainty and GPU-based parallel repair approach. *Expert Systems with Applications*, 129544.
- Ramazan, S., Dagdelen, K., Johnson, T.B., (2005). Fundamental tree algorithm in optimising production scheduling for open pit mine design. *Inst. Min. Metall. Trans. Sect. A Min. Technol.* 114 (1), 45–54. <https://doi.org/10.1179/037178405X44511>.
- Ramazan, S., (2007). The new fundamental tree algorithm for production scheduling of open pit mines. *Eur. J. Oper. Res.* 177 (2), 1153–1166.
- Rimélé, A., Dimitrakopoulos, R., & Gamache, M. (2020). A dynamic stochastic programming approach for open-pit mine planning with geological and commodity price uncertainty. *Resources Policy*, 65, 101570.
- Sari, Y.A., Kumral, M., (2016). An improved meta-heuristic approach to extraction sequencing and block routing. *J. South Afr. Inst. Min. Metall.* 116 (7), 673–680. <https://doi.org/10.17159/2411-9717/2016/v116n7a9>.
- Soleymani Shishvan, M., Sattarvand, J., Feb. (2015). Long term production planning of open pit mines by ant colony optimisation . *Eur. J. Oper. Res.* 240, 825–836. <https://doi.org/10.1016/j.ejor.2014.07.040>.

- Tolouei, K., Moosavi, E., Bangian Tabrizi, A.H., Afzal, P., (2020a). Application of an improved Lagrangian relaxation approach in the constrained long-term production scheduling problem under grade uncertainty. *Eng. Optim.* <https://doi.org/10.1080/0305215X.2020.1746295> vol. 0273.
- Tolouei, K., Moosavi, E., Tabrizi, A.H.B., Afzal, P., Bazzazi, A.A., (2020b). An optimisation approach for uncertainty-based long-term production scheduling in open-pit mines using meta-heuristic algorithms. *Int. J. Min. Reclamat. Environ.* 1–26. <https://doi.org/10.1080/17480930.2020.1773119> vol. 00, no. 00.
- Tolouei, K., Moosavi, E., Bangian Tabrizi, A.H., Afzal, P., Aghajani Bazzazi, A., (2020c). Improving performance of open-pit mine production scheduling problem under grade uncertainty by hybrid algorithms. *J. Cent. South Univ.* 27 (9), 2479–2493. <https://doi.org/10.1007/s11771-020-4474-z>.
- Tolouei, K., Moosavi, E., Tabrizi, A. H. B., Afzal, P., & Bazzazi, A. A. (2021). An optimisation approach for uncertainty-based long-term production scheduling in open-pit mines using meta-heuristic algorithms. *International Journal of Mining, Reclamation and Environment*, 35(2), 115–140.
- Upadhyay, S. P., & Askari-Nasab, H. (2018). Simulation and optimisation approach for uncertainty-based short-term planning in open pit mines. *International Journal of Mining Science and Technology*, 28(2), 153-166.